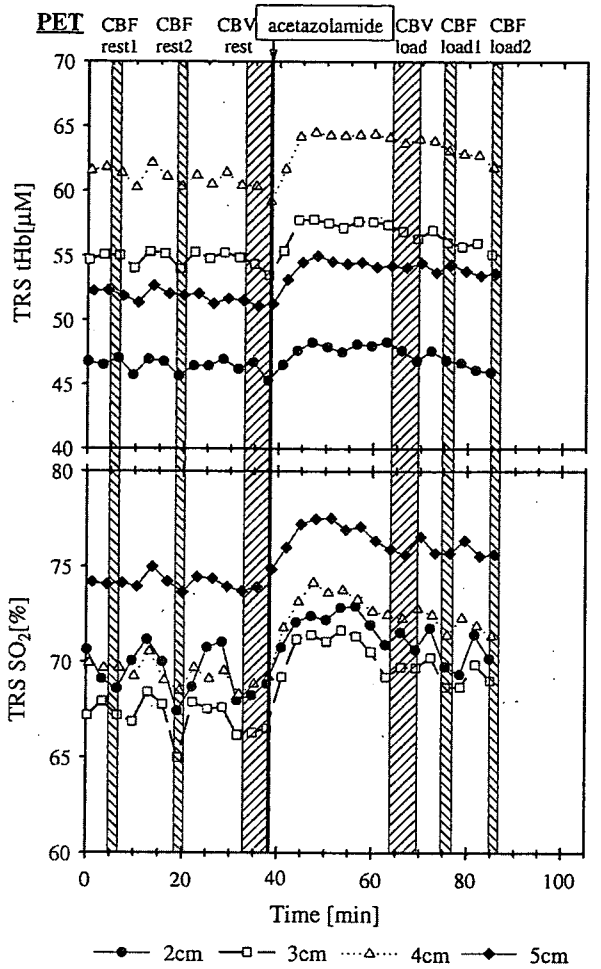

Fig. 4. TRS measurement results at each optode spacing. Typical responses (41 years old; male) of TRS tHb (upper) and SO_2 (lower) for acetazolamide administration. The oblique lines indicate PET data acquisition period.

state significantly rose approximately 6% and 3%, respectively, of resting state at all optode spacing.

PET

The CBF and CBV images at the resting and loading state are shown in Fig. 2B. The CBF can be clearly seen to increase after administering acetazolamide, whereas the CBV shows a relatively minor increase.

Mean values of PET CBF and PET CBV at each VOI in the rest and loading state are shown in Fig. 6. The PET CBF and PET CBV at each VOI in the resting state were as follows: VOI_1 (arbitrary unit): 6.6 ± 1.2 cm^3/100 g/min, 2.6 ± 0.4 cm^3/100 g, VOI_2: 39.6 ± 5.3 cm^3/100 g/min, 4.4 ± 0.9 cm^3/100 g, VOI_3: 40.6 ± 5.1 cm^3/100 g/min, 4.0 ± 0.7 cm^3/100 g. The PET CBF and PET CBV at $VOI_{2,3}$ in the loading state significantly increased approximately 30% and 10%, respectively, compared to those of resting state. However, no significant increases were observed for the CBF and CBV at VOI_1, which increased 8.2% and −1.3%, respectively.

Correlations

The r^2 for the CBV and ΔCBV, respectively, between TRS and PET are shown in Tables 1A and B.

The r^2 of CBV at 4 cm and 5 cm of optode spacing was higher than those at 2 cm and 3 cm of optode spacing at all VOI, and they also showed high correlation values as the depth increased.

As to ΔCBV, r^2 of VOI_2 showed exceptionally higher than those of VOI_3 at all optode spacing. At the VOI_2, however, r^2 at 2 cm of optode spacing showed lower than those at other optode spacing. At the VOI_3, just as with the CBV correlation, r^2 at 4 cm and 5 cm of optode spacing showed higher than those at 2 cm and 3 cm of optode spacing.

L_{ext} and the contribution ratio

L_{ext} at each wavelength was as follows: 761 nm 11.7 ± 2.7 cm, 791 nm: 6.3 ± 2.4 cm, 836 nm: 6.5 ± 1.5 cm. L_{ext} at 761 nm was significantly longer than those of 791 and 836 nm, against

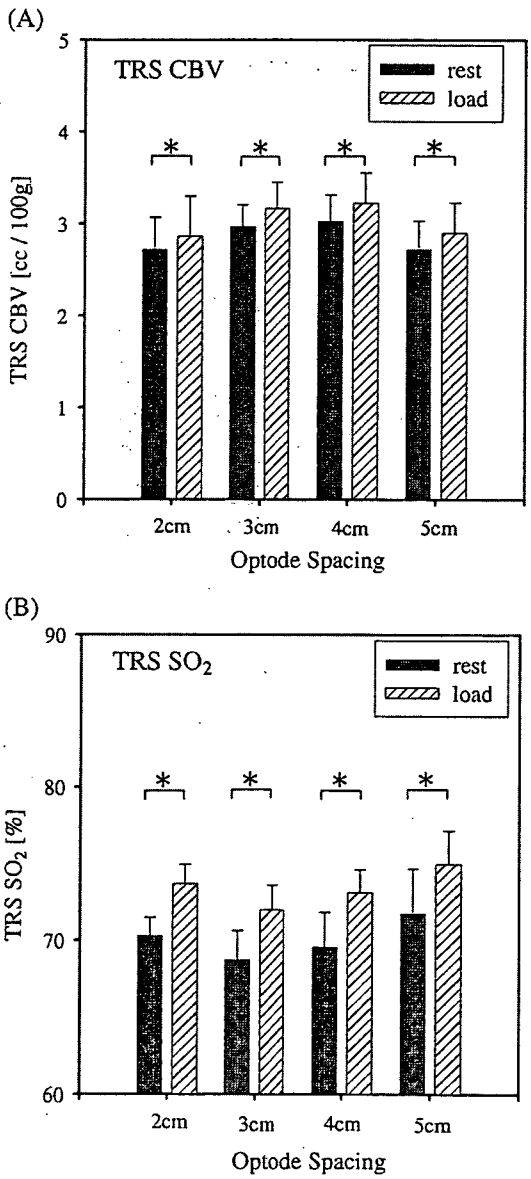

Fig. 5. Mean values (n = 6) for (A) TRS CBV and (B) SO_2 in the resting and loading state. Significant differences were confirmed for all optode spacings after administering acetazolamide (*P < 0.05).

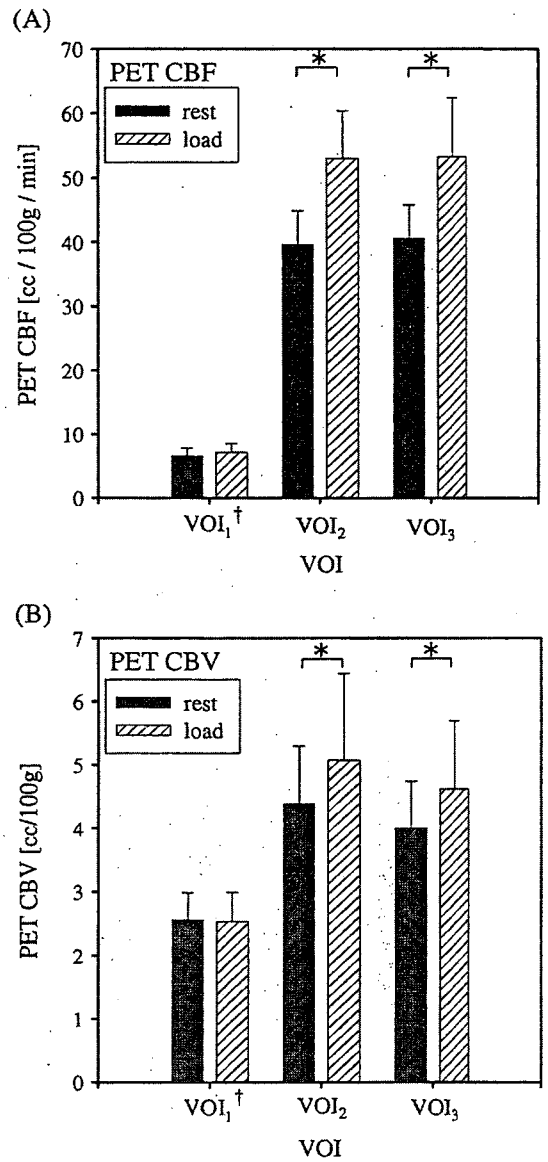

Fig. 6. Mean values (n = 6) for (A) PET CBF and (B) PET CBV in the resting and loading state. Significant differences were confirmed at VOI_2 and VOI_3 after administering acetazolamide (*P < 0.05). †VOI_1 was expressed in the arbitrary unit.

observed mean pathlength of each wavelengths were also the same (data is not shown).

The contribution ratios of the cerebral tissue at each wavelength are shown in Fig. 7. The contribution ratios of 761 nm with all optode spacing were significantly lower than those of 791 and 836 nm.

Discussion

The acetazolamide used in this experiment increases the regional CBF by inhibiting carbonic anhydrase and thereby expanding cerebral blood vessels (Posner and Plum, 1960; Ehrenreich et al., 1961). This drug is therefore generally used to assess the cerebrovascular reserve capacity as an acetazolamide test. Similarly in this study, significant increases of PET CBF and PET CBV by

Table 1
Squared correlation coefficient (r^2) between PET and TRS: (A) CBV; (B) ΔCBV

TRS optode spacing	PET	
	VOI_2	VOI_3
(A) r^2: TRS CBV vs. PET CBV (n = 6)		
2 cm	0.601**	0.535**
3 cm	0.410*	0.525**
4 cm	0.690**	0.841**
5 cm	0.762**	0.859**
(B) r^2: TRS ΔCBV vs. PET ΔCBV (n = 6)		
2 cm	0.331	0.050
3 cm	0.633*	0.277
4 cm	0.699*	0.457
5 cm	0.585	0.352

* $P < 0.05$.
** $P < 0.01$.

acetazolamide in the intracerebral tissues ($VOI_{2,3}$) and no significant increase of those in the extracerebral tissues (VOI_1) were confirmed. In the TRS measurements on the other hand, significant increases in CBV at all optode spacings were observed. Further, the result of significant increases of SO_2 at all optode spacing agrees well with a report (Vorstrup et al., 1984) that there was hardly any change in $CMRO_2$ even though the CBF increased when acetazolamide was administered. These results suggest that when optode spacing is 2 cm to 5 cm, the photons passing through the head convey the intracerebral hemodynamic response.

However, the CBV and ΔCBV correlations clearly differed according to the optode spacing and VOI. As for CBV correlation, these trends suggest that the longer the optode spacing, the deeper the region that the photons can penetrate, because the correlation with VOI_3 was higher than that with VOI_2 at each optode spacing except at 2 cm. In addition, correlations at 4 cm and 5 cm of optode spacing showed a trend to higher than those at 2 cm and 3 cm of optode spacing with both VOIs. These results suggested that optode spacing was preferably more than 4 cm for improving quantification of NIR-TRS to cerebral hemodynamics.

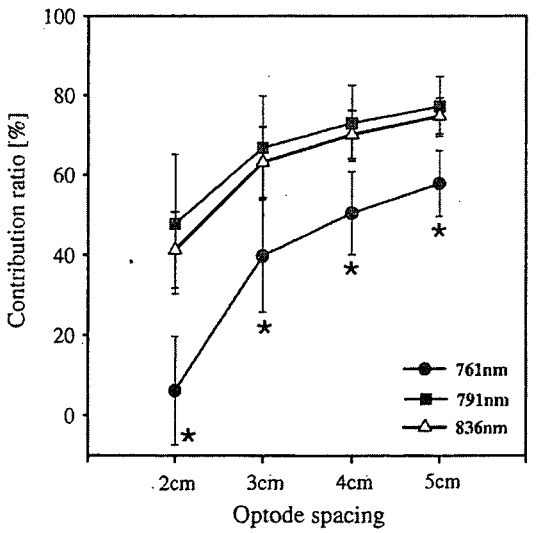

Fig. 7. Mean values (n = 5) for contribution rations of the cerebral tissue to observed absorption change. Significant differences were confirmed for all optode spacing at 761 nm to 791 and 836 nm (*P < 0.05).

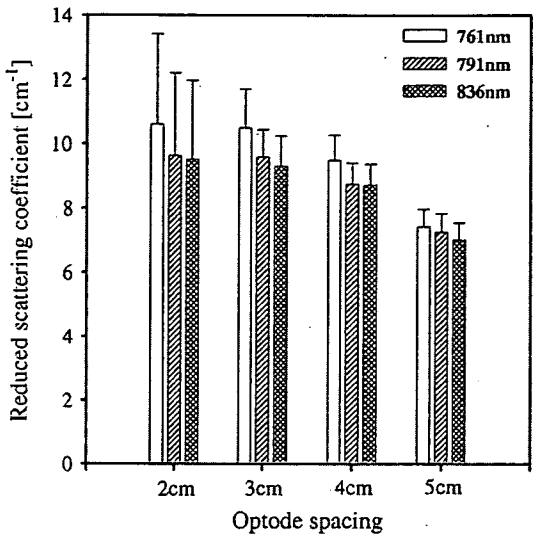

Fig. 8. Mean values (n = 5) for reduced scattering coefficient at each wavelength and optode spacing. The values of 761 nm for all optode spacing were highest among three wavelengths (no significant differences).

Because the density of blood vessels in VOI_2, which covers the gray matter mostly, was high, there might be a large increase in blood volume. Accordingly, the ΔCBV correlation with VOI_2 may be higher than VOI_3 regardless of the optode spacing. Also, the ΔCBV correlation for VOI_2 is a maximum at 4 cm of optode spacing so that this distance may be optimum for capturing cerebral hemodynamics response around the gray matter region.

Contribution ratios at 4 cm of optode spacing were as follows: 761 nm: 50.4 ± 10.3%, 791 nm: 72.9 ± 9.4%, 836 nm: 70.0 ± 6.0%. The results at 836 nm are very much in agreement with the results at 834 nm by Kohri (Kohri et al., 2001). But these results are different from previous simulation work (Firbank et al., 1995). The photon propagation depends heavily on the optical parameters of tissues. We believe that the μ_a and μ_s' of the postmortem adult human brain (Van der Zee et al., 1992) and piglet (Firbank et al., 1993) used in the simulation work maybe different from those in living tissues. Furthermore, both contribution ratios at 5 cm of optode spacing were higher than those at 4 cm and the ΔCBV correlation at 5 cm of optode spacing is lower than that at 4 cm; thus it is speculated that photons has penetrated even deeper, and contains information not only on gray matter but also on white matter and cerebral ventricle. Conversely, the lowest value of the ΔCBV correlation at 2 cm of optode spacing corresponds with derived low contribution ratios. So the 2 cm of optode spacing is not recommended for acquiring intracerebral information. Although we treated a complex layered structure as a single set of μ_a and μ_s', assuming of a homogeneous medium, making optode spacing longer could satisfy this condition concededly.

L_{cxt} at 761 nm was 1.7 times of those at 791 and 836 nm, although observed mean pathlength at each wavelength was also the same values. It means that the photons of 761 nm are hard to penetrate into the cerebral tissue than those of 791 and 836 nm. To support this result, mean values for μ_s' at each wavelength and the optode spacing in the resting state are shown in Fig. 8. As the higher the scattering, the photons are harder to spread into the cerebral tissue deeply. The difference of μ_s' among wavelength showed a similar tendency to that of L_{ext}. It was also reported that the value of μ_s' increases progressively with decreasing wavelength (Bevilacqua et al., 1999; Torricelli et al., 2001). To improve the accuracy of NIR measurement, it should be necessary to consider wavelength selection including μ_s' as well as absorption spectra of hemoglobin.

The TRS system has a potential to quantitate the hemoglobin concentration since it directly measures the optical pathlength distribution of detected photons passing through the living tissue, different from the conventional measurement methods (Brazy et al., 1985; Ferrari et al., 1987; Cope and Delpy, 1988). This allows making patient-to-patient comparisons and comparing the patient condition before and after treatment, making it highly valuable as an indicator for diagnosis and treatment. In this study, a good correlation coefficient was obtained between TRS-derived CBV and PET-derived CBV, while the absolute CBV levels by TRS were lower than those by PET. One reason for the under-/over-estimation of the CBV values might be a difference in modalities which measure different in vivo responses. An absolute value of CBV weighs considerably in the NIRS study. Thus, further studies are needed to resolve this methodological issue.

NIR measurement is proven capable of continuous measurement with high time resolution while also being a simple, safe and non-invasive method. Additionally, study of diffuse optical tomography is being proceeded based on this technology (Ueda et al., 2001; Hillman et al., 2001). We hope to further develop our work in the NIRS field to the level where it can be used as a modality to assist and complement PET technology.

Conclusion

We observed a change in the CBV by administration of acetazolamide with simultaneous measurement of TRS and PET. These experiments showed that intracerebral hemodynamics response by administering acetazolamide could be captured at optode spacings of 2 cm to 5 cm.

Furthermore, by evaluating the correlation with PET, we concluded that more than 4 cm of optode spacing is preferable for improving quantification of the NIR-TRS measurement to intracerebral hemodynamics. Additionally, 4 cm of optode spacing is a good setting to monitor cerebral hemodynamics response around the gray matter region. Contribution ratio of intracerebral tissue at 4 cm estimated about 70%, although it varies according to wavelength. NIR measurement is a simple and easy method to evaluate cerebral hemodynamics.

Acknowledgments

The authors would like to thank Mr. T. Hiruma for his constant support and encouragement. The authors are also grateful to Drs. Y. Tsuchiya and T. Yamashita for useful discussions.

Appendix A. Derive reduced scattering and absorption coefficients from temporal profiles

Behavior of photon within scattering and absorption media like a living body is expressed by the photon diffusion Eq. (1) (Patterson et al., 1989).

$$\frac{1}{v}\frac{\partial}{\partial t}\phi(r,t) - D\nabla^2\phi(r,t) + \mu_a\varphi(r,t) = S(r,t) \quad (1)$$

where $\phi(r, t)$ is the diffuse photon fluence rate at position r and time t, D is the photon diffusion coefficient and expressed in $D = 1/3\mu_s'$, v is the velocity of light within the media and $S(r, t)$ is the light source.

Solutions using this equation are found under different boundary conditions. We used the solution of a semi-infinite homogeneous model (Patterson et al., 1989) for TRS data analysis. In this solution, $R(d, t)$ is expressed by a function of the optode spacing, the reduced scattering coefficient (μ_s') and absorption coefficient (μ_a), as shown in Eq. (2).

$$R(d,t) = (4\pi Dv)^{-\frac{3}{2}} z_0 t^{-\frac{5}{2}} \exp(-\mu_a vt) \exp\left(-\frac{d^2 + z_0^2}{4Dvt}\right) \tag{2}$$

where d is the optode spacing and $z_0 = 1/\mu_s'$.

Using the non-linear least squares method, we fit Eq. (2) into the observed temporal profiles obtained from TRS and determined μ_s' and μ_a at each wavelength (Suzuki et al., 1994). The conversion chi-square (χ_v^2) value was adopted to evaluate fitting accuracy. We confirmed that our observed profiles fitted well with the theoretical curves using this index ($0.8 < \chi_v^2 < 1.2$; Grinvald and Steinberg, 1974).

Appendix B. Calculation of hemoglobin concentration and oxygen saturation by absorption coefficients

The μ_a of the 3 wavelengths (761, 791, 836 nm) that were measured is expressed as shown in simultaneous Eq. (3).

$$\begin{aligned}
\mu_{a761nm} &= \varepsilon_{oxyHb761nm} C_{oxyHb} + \varepsilon_{deoxyHb761nm} C_{deoxyHb} \\
&\quad + \varepsilon_{H_2O761nm} C_{H_2O} + \mu_{abkg761nm} \\
\mu_{a791nm} &= \varepsilon_{oxyHb791nm} C_{oxyHb} + \varepsilon_{deoxyHb791nm} C_{deoxyHb} \\
&\quad + \varepsilon_{H_2O791nm} C_{H_2O} + \mu_{abkg791nm} \\
\mu_{a836nm} &= \varepsilon_{oxyHb836nm} C_{oxyHb} + \varepsilon_{deoxyHb836nm} C_{deoxyHb} \\
&\quad + \varepsilon_{H_2O836nm} C_{H_2O} + \mu_{abkg836nm}
\end{aligned} \tag{3}$$

where μ_a is the absorption coefficient at the wavelength λ, $\varepsilon_{m\lambda}$ is the molar extinction coefficient of the substance m at the wavelength λ, C_m is the concentration of the substance m and bkg is the chromophores contributing to μ_a in tissue for other than oxygenated hemoglobin (oxyHb), deoxygenated hemoglobin (deoxyHb) and water.

Based on the assumption that light absorption in the living body in this wavelength region occurs from oxyHb, deoxyHb and water, and also that there is no other background absorption in the living body (Tromberg et al., 1997), we determined TRS values for oxygenated hemoglobin (TRS HbO_2) and deoxygenated hemoglobin (TRS Hb) as tissue water concentration is 70%.

TRS total hemoglobin (TRS tHb) and SO_2 were obtained from Eq. (4) as follows.

$$\text{TRS tHb}[\mu M] = \text{TRS HbO}_2 + \text{TRS Hb},$$

$$SO_2[\%] = \frac{\text{TRS HbO}_2}{\text{TRS tHb}} \times 100 \tag{4}$$

Appendix C. Conversion TRS tHb into TRS CBV

We converted the TRS tHb into the CBV by TRS (TRS CBV) using Eq. (5) (Wyatt et al., 1990) for comparison with the CBV by PET (PET CBV).

$$\text{TRS CBV}[\text{cc}/100\text{ g}] = \frac{\text{TRS tHb} \times MW_{Hb}}{Hb \times \eta \times \rho \times 100000} \tag{5}$$

where MW_{Hb} is hemoglobin molecular weight; 64,500, Hb is arterial hemoglobin concentration (g/dl) of subject, η is the cerebral-to-large-vessel hematocrit ratio; 0.85 (Phelps et al., 1979) and ρ is density of cerebral tissue (g/ml); 1.04 (Picozzi et al., 1985).

References

Bevilacqua, F., Piguet, D., Marquet, P., Gross, J.D., Tromberg, B.J., Depeursinge, C., 1999. In vivo local determination of tissue optical properties: applications to human brain. Appl. Opt. 38 (22), 4839–4950.

Brazy, J.E., Lewis, D.V., Mitnick, M.H., Jobsis, F.F., 1985. Noninvasive monitoring of cerebral oxygenation in preterm infants: preliminary observations. Pediatrics 75, 217–225.

Cope, M., Delpy, D.T., 1988. A system for long-term measurement of cerebral blood and tissue oxygenation in newborn infants by near infrared transillumination. Med. Biol. Eng. Comput. 26, 289–294.

De Blasi, R.A., Almenräder, N., Ferrari, M., 1997. Brain oxygenation monitoring during cardiopulmonary bypass by near infrared spectroscopy. Adv. Exp. Med. Biol. 413, 97–104.

Ehrenreich, D.L., Burns, R.A., Alman, R.W., Fazekas, J.F., 1961. Influence of acetazolamide on cerebral blood flow. Arch. Neurol. 5, 227–232.

Ferrari, M., Zanette, E., Sideri, G., Gianni, I., Fieschi, C., Carpi, A., 1987. Effects of carotid compression, as assessed by near infrared spectroscopy, upon cerebral volume and haemoglobin oxygen saturation. J. R. Soc. Med. 80, 83–87.

Firbank, M., Hiraoka, M., Essebpreis, M., Delpy, D.T., 1993. Measurement of the optical properties of the skull in the wavelength range 650–950 nm. Phys. Med. Biol. 38, 503–510.

Firbank, M., Schweiger, M., Delpy, D.T., 1995. Investigation of 'light piping' through clear regions of scattering objects. SPIE 2389, 167–173.

Germon, T.J., Evans, P., Barnett, N., Wall, P., Nelson, R.J., 1995. Optode separation determines sensitivity of near infrared spectroscopy to intra- and -external oxygenation changes. J. Cereb. Blood Flow Metab. 15, 617.

Grinvald, A., Steinberg, I.Z., 1974. On the analysis of fluorescence decay kinetics by the method of least-squares. Anal. Biochem. 59 (5), 583–598.

Harris, D.N.F., Cowans, F.M., Wertheim, D.A., Hamid, S., 1994. NIRS in adult-effects of increasing optode separation. Adv. Exp. Med. Biol. 345, 837–840.

Herscovitch, P., Markham, J., Raichle, M.E., 1983. Brain blood flow measured with intravenous H215O: I. Theory and error analysis. J. Nucl. Med. 24, 782–789.

Hillman, E., Hebden, J., Schweiger, M., Dehghani, H., Schmidt, F.E.W., Delpy, D.T., Arridge, S.R., 2001. Time resolved optical tomography of the human forearm. Phys. Med. Biol. 46, 1117–1130.

Isobe, K., Kusaka, T., Fujikawa, Y., Kondo, M., Yasuda, S., Itoh, S., Hirano, K., Onishi, S., 2000. Changes in cerebral hemoglobin concentration and oxygen saturation immediately after birth in the human neonate using full-spectrum near infrared spectroscopy. J. Biomed. Opt. 5 (3), 283–286.

Iwai, H., Urakami, T., Miwa, M., Nishizawa, M., Tsuchiya, Y., 2001. Tissue spectroscopy with a newly developed phase modulation system based on the microscopic Beer-Lambert law. SPIE 4250, 482–488.

Iwase, M., Ouchi, Y., Okada, H., Yokoyama, C., Nobezawa, S., Yoshikawa, E., Tsukada, H., Takeda, M., Yamashita, K., Takeda, M., Yamaguti, K., Kuratsune, H., Shimizu, A., Watanabe, Y., 2002. Neural substrates of human facial expression of pleasant emotion induced by comic films: a PET study. NeuroImage 17, 758–768.

Jobsis, F.F., 1977. Noninvasive, infrared monitoring of cerebral and myocardial oxygen sufficiency and circulatory parameters. Science 198, 1264–1267.

Kakihana, Y., Matsunaga, A., Yamada, H., Dohgomori, H., Oda, T., Yoshimura, N., 1996. Continuous, noninvasive measurement of cytochrome oxidase in cerebral cortex by near-infrared spectrophotometry during aortic arch surgery. J. Anesth. 10, 221–224.

Kohri, S., Hoshi, Y., Tamura, M., Kato, C., Kuge, Y., Tamaki, N., 2001. Quantitative evaluation of the relative contribution ratio of cerebral tissue to near-infrared signals in adult human head. A preliminary study. Physiol. Meas. 23 (2), 301–312.

Lammertsma, A.A., Jones, T., 1983. Correction for the presence of intravascular oxygen-15 in the steady-state technique for measuring regional oxygen extraction ratio in the brain: 1. Description of the method. J. Cereb. Blood Flow Metab. 3, 416–424.

Lammertsma, A.A., Baron, J.C., Jones, T., 1987. Correction for intravascular activity in the oxygen-15 steady-state technique is independent of the regional hematocrit. J. Cereb. Blood Flow Metab. 7, 372–374.

McCormick, P.W., Stewart, M., Lewis, G., Dujovny, M., Ausman, J.I., 1992. Intracerebral penetration of infrared light. J. Neurosurg. 76 (2), 315–319.

Meek, J.H., Elwell, C.E., McCormick, D.C., Edwards, A.D., Townsend, J.P., Stewart, A.L., Wyatt, J.S., 1999. Abnormal cerebral haemodynamics in perinatally asphyxiated neonates related to outcome. Arch. Dis. Child., Fetal Neonatal Ed. 81 (2), F110–F115 (Sep).

Misonoo, S., Okada, E., 2001. Adult head modeling based on time-resolved measurement for NIR instrument. SPIE 4250, 522–529.

Oda, M., Yamashita, Y., Nishimura, G., Tamura, M., 1996. A simple and novel algorithm for time-resolved multiwavelength oximetry. Phys. Med. Biol. 41, 551–562.

Oda, M., Nakano, T., Suzuki, A., Shimizu, K., Hirano, I., Shimomura, F., Ohmae, E., Suzuki, T., Yamashita, Y., 2000. Nearinfrared time-resolved spectroscopy system for tissue oxygenation monitor. SPIE 4160, 204–210.

Okada, E., Delpy, D.T., 2000. Effects of scattering of arachnoid trabeculae on light propagation in the adult brain. Advances in optical imaging, photon migration, and tissue optics. OSA Tech. Dig. 256–258.

Okada, E., Delpy, D.T., 2003a. Near-infrared light propagation in an adult head model: I. Modeling of low-level scattering in the cerebrospinal fluid layer. Appl. Opt. 42 (16), 2906–2914.

Okada, E., Delpy, D.T., 2003b. Near-infrared light propagation in an adult head model: II. Effect of superficial tissue thickness on the sensitivity of the near-infrared spectroscopy signal. Appl. Opt. 42 (16), 2915–2922.

Okada, E., Firbank, M., Schweiger, M., Arridge, S.R., Cope, M., Delpy, D.T., 1997. Theoretical and experimental investigation of near-infrared light propagation in a model of the adult head. Appl. Opt. 36 (1), 21–31.

Ouchi, Y., Nobezawa, S., Okada, H., Yoshikawa, E., Futatsubashi, M., Kaneko, M., 1998. Altered glucose metabolism in the hippocampal head in memory impairment. Neurology 51, 136–142.

Ouchi, Y., Okada, H., Yoshikawa, E., Futatsubashi, M., Nobezawa, S., 2001. Absolute changes in regional cerebral blood flow in association with upright posture in humans: an orthostatic PET study. J. Nucl. Med. 42, 707–712.

Patterson, M.S., Chance, B., Wilson, B.C., 1989. Time resolved reflectance and transmittance for the noninvasive measurement of tissue optical properties. Appl. Opt. 28 (12), 2331–2336.

Phelps, M.E., Huang, S.C., Hoffman, E.J., Kuhl, D.E., 1979. Validation of tomographic measurement of cerebral blood volume with C-11-labeled carboxyhemoglobin. J. Nucl. Med. 20, 328–334.

Picozzi, P., Todd, N.V., Crockard, A.H., 1985. The role of cerebral blood volume changes in brain specific-gravity measurements. J. Neurosurg. 62 (5), 704–710 (May).

Posner, J.P., Plum, F., 1960. The toxic effects of carbon dioxide and acetazolamide in hepatic encephalopathy. J. Clin. Invest. 39, 1246–1258.

Suzuki, K., Yamashita, Y., Ohta, K., Chance, B., 1994. Quantitative measurement of optical parameters in the breast using time-resolved spectroscopy. Invest. Radiol. 29 (4), 410–414.

Suzuki, S., Takasaki, S., Ozaki, T., Kobayashi, Y., 1999. A tissue oxygenation monitor using NIR spatially resolves spectroscopy. SPIE 3597, 582–592.

Tanosaki, M., Hoshi, Y., Iguchi, Y., Oikawa, Y., Oda, I., Oda, M., 2001. Variation of temporal characteristics in human cerebral hemodynamic responses to electric median nerve stimulation: a near-infrared spectroscopic study. Neurosci. Lett. 316, 75–78.

Torricelli, A., Pifferi, A., Taroni, P., Giambattistelli, E., Cubeddu, R., 2001. In vivo optical characterization of human tissues from 610 to 1010 nm by time-resolved reflectance spectroscopy. Phys. Med. Biol. 46, 2227–2237.

Tromberg, B.J., Coquoz, O., Fishkin, J.B., Pham, T., Anderson, E., Butler, J., Cahn, M., Gross, J.D., Venugopalan, V., Pham, D., 1997. Noninvasive measurements of breast tissue optical properties using frequency-domain photon migration. Philos. Trans. R. Soc. Lond., B 352, 661–668.

Tuchiya, Y., Urakami, T., 1996. Frequency domain analysis of photon migration based on the microscopic Beer-Lambert law. Jpn. J. Appl. Phys. 35, 4848–4851.

Ueda, U., Ohta, K., Oda, M., Miwa, M., Tsuchiya, Y., Yamashita, Y., 2001. 3-D imaging of a tissue-like phantom by diffusion optical tomography. Appl. Opt. 40 (34), 6349–6355.

Van der Zee, P., Cope, M., Arridge, S.R., Essenpreis, M., Potter, L.A., Edwards, A.D., Wyatt, J.S., McCormick, D.C., Roth, S.C., Reynolds, E.O.R., Delpy, D.T., 1992. Experimentally measured optical pathlength for the adult head, calf and forearm and the head of the newborn infant as a function of inter optode spacing. Exp. Med. Biol. 316, 143–153.

Vorstrup, S., Henriksen, L., Paulson, O., 1984. Effect of acetazolamide on cerebral blood flow and cerebral metabolic rate for oxygen. J. Clic. Invest. 74, 1634–1639.

Watanabe, E., Maki, A., Kawaguchi, F., Yamashita, Y., Koizumi, H., Mayanagi, Y., 2000. Noninvasive cerebral blood volume measurement during seizures using multichannel near infrared spectroscopic topography. J. Biomed. Opt. 5 (3), 287–290.

Wyatt, J.S., Cope, M., Delpy, D.T., Richardson, C.E., Edwards, A.D., Wray, S., Reynolds, E.O.R., 1990. Quantitation of cerebral blood volume in human infants by near-infrared spectroscopy. J. Appl. Physiol. 68, 1086–1091.

Yamashita, Y., Oda, M., Ohmae, E., Tamura, M., 1998. Continuous measurement of oxy- and deoxyhemoglobin of piglet brain by time-resolved spectroscopy. OSA TOPS 22, 205–207.

Zhang, H., Miwa, M., Urakami, T., Yamashita, Y., Tsuchiya, Y., 1998. Simple subtraction method for determining the mean path length traveled by photons in turbid media. Jpn. J. Appl. Phys. 37, 700–704.

Available online at www.sciencedirect.com
ScienceDirect
Neuroscience Letters 407 (2006) 131–135
Neuroscience Letters
www.elsevier.com/locate/neulet

Changes in cerebral blood flow under the prone condition with and without massage

Yasuomi Ouchi [a,*], Toshihiko Kanno [a], Hiroyuki Okada [b], Etsuji Yoshikawa [b], Tomomi Shinke [b], Shingo Nagasawa [c], Keiji Minoda [d], Hiroyuki Doi [e]

[a] *Positron Medical Center, Hamamatsu Medical Center, 5000 Hirakuchi, Hamamatsu 434-0041, Japan*
[b] *Central Research Laboratory, Hamamatsu Photonics K.K., Hamamatsu, Japan*
[c] *Yanaihara Laboratory, Fuji, Japan*
[d] *Balance Therapy University, Fukuoka, Japan*
[e] *Shizuoka Prefectural Government, Shizuoka, Japan*

Received 17 May 2006; received in revised form 25 July 2006; accepted 10 August 2006

Abstract

To investigate changes in regional cerebral blood flow (rCBF) under the prone condition with and without light massage on the back, we measured rCBF quantitatively in healthy human subjects using positron emission tomography with $H_2{}^{15}O$. Biochemical tests showed that the light massage (palm-pressure) reduced levels of stress-related serum cortisol and salivary stress protein chromogranin-A measured after the PET examination. Absolute rCBF significantly increased in the parietal cortex (precuneus) under the prone condition compared with the supine condition, and this rCBF increase was in parallel with comfortable sensation and slowing heart rate during the massage. Correlation analysis in statistical parametric mapping showed that the amygdalar and basal forebrain rCBF correlated with parasympathetic function (heart rate reduction), indicating involvement of the forebrain-amygdala system in mediating activities in the autonomic nervous system in the presence of comfortable sensation. To conclude, prone posture itself can stimulate the precuneus region to raise awareness, and the light massage on the back may help accommodate the brain to comfortable stimulation.

Keywords: Prone posture; Palm-pressure massage; Cerebral blood flow; Positron emission tomography; Precuneus

A prone posture is what people sometimes assume for a quick rest in the daily living and is a common style during massage therapy. It is well accepted that massage therapy gives positive effects on physical and mental care irrespective of health conditions [4,18,23]. Specifically, moderate pressure massage is reported to cause reductions in heart rate and in alpha and beta activities on electroencephalography (EEG), indicating generation of a relaxation response [23]. Biochemical basic studies also indicated massage-related favorable changes in the immune [8] and neurohormonal systems [22]. Thus, we hypothesized that the maneuver could alter brain activity in a specific region that relates to autonomic nervous system.

Exploration of brain activation can be achieved by using neuroimaging techniques such as positron emission tomography (PET) and functional magnetic resonance imaging (fMRI) in the field of complementary alternative medicine, e.g. acupuncture [2,13]. We have recently developed a new imaging method that enables to scan human subjects on the prone condition using PET [16]. This technique allows us to investigate the effect of back massage on regional cerebral blood flow (rCBF) quantitatively. Previous studies indicate that the inferomedial region of the frontal cortex and amygdala are likely to play central roles in relaxation processing [11,14] and that the precuneus engages in the integration of multiple neural systems producing a conscious self-percept [1]. Thus, the purpose of the present study was to examine absolute changes in rCBF in the prone posture with and without massage applied on the back using PET with $H_2{}^{15}O$.

Eight right-handed healthy volunteers (4 male, 4 female; mean age ± S.D., 40.2 ± 10.7 years) participated in the current study. All participants had neither neurological problems nor habits of regular intake of over-the-counter pills, and were naïve

* Corresponding author. Tel.: +81 53 585 0366; fax: +81 53 585 0367.
E-mail address: ouchi@pmc.hmedc.or.jp (Y. Ouchi).

0304-3940/$ – see front matter © 2006 Published by Elsevier Ireland Ltd.
doi:10.1016/j.neulet.2006.08.037

to the current palm-pressure massage. The present study was approved by the Ethics Committee of the Hamamatsu Medical Center, and written informed consent was obtained from all participants. To examine stress neuroendocrinologically, we measured salivary levels of chromogranin-A, a protein induced by mental stress [10,15] and cortisol in blood [20] before and after the measurement.

Three-dimensional MRI by a 0.3 T scanner (MRP7000AD, Hitachi, Tokyo, Japan) revealed no morphological abnormalities. Then, a maximum of four to six PET scans were performed under the following conditions with all eyes closed; (a) supine at rest, (b) prone at rest, (c) prone with back massage at an early stage (4 min after the stimulation, Stim-1), (d) prone with back massage at a later stage (20 min after the stimulation, Stim-2). The massage was performed in a similar manner over the back target region. Two professional therapists from Balance Therapy University performed palm-pressure massage onto the back muscles including trapezius, rhombodeus and latissimus dorsi for nearly 24 min, consecutively.

Using a brain-purpose PET scanner (SHR12000, Hamamatsu Photonics, Hamamatsu, Japan), we performed quantitative measurement of rCBF in a conventional way [7,17] but in a different condition in which arterial blood was sampled continuously through the catheter inserted in the left brachial artery while the examinee was lying on his/her stomach during the PET scan. The dose of $H_2{}^{15}O$ injected was set 300 MBq/scan for each measurement. To establish the reproducible measurement under the prone posture, we used a thermoplastic facemask attached firmly to the scanner's couch during the prone condition, which allowed the volunteer to be secured in the gantry and to avoid misregistration artifacts [16]. The heart rate, arterial blood pressure and skin temperature were monitored simultaneously during scans. The subjective visual analog scale (VAS) for relaxation (ranging from 1 to 10, 1 being the most uncomfortable to 10 being the most comfortable) was rated after each PET scan.

Each rCBF value was calculated based on a region of interest (ROI) method, in which semicircular ROIs were placed over the cerebellum, lower frontal area (Brodmann area or BA: 10/11), upper frontal area (BA: 6/8), temporal (BA: 21/22), parietal (BA: 7), occipital (BA: 17/18) cortices, the striatum and the thalamus on the MR images and the corresponding PET images [16]. Repeated measures analysis of variance (ANOVA) was used for analyzing changes in rCBF among the present conditions. Following a Bonferroni post hoc test, a p-value less than 0.05 was regarded as statistically significant. In addition, we performed a voxel-wise mapping analysis using SPM2 (Wellcome Department of Cognitive Neurology, University College, London) to elucidate brain loci significantly activated during the massage. Voxel-based correlations were computed between physiological parameters and rCBF using VAS scores as confounding covariates, and the statistical threshold was set at $p = 0.001$ uncorrected for peak height and at clusters over 50 contiguous voxels.

Among physiological parameters, a significant reduction was observed only in heart rate during the Stim-2 condition (Table 1, Fig. 1D). The χ^2-test disclosed that the concentrations of salivary chromogranin-A and plasma cortisol were significantly lower after PET examination (0.8 ± 1.0 pmol/mg-protein

Table 1
Results of physiology and cerebral blood flow during each condition

Condition	Physiology			Cerebral blood flow (ml/100g/min)							
	MABP (mmHg)	Heart rate (b/m)	Temperature (°C)	Cerebellum	Lower frontal	Upper frontal	Temporal	Parietal	Occipital	Thalamus	Striatum
Supine	81.1 ± 8.3	71.2 ± 9.8	N.E.	51.1 ± 7.3	45.4 ± 5.9	50.0 ± 6.2	49.9 ± 4.9	49.3 ± 6.4	46.5 ± 7.2	54.5 ± 6.8	56.8 ± 8.3
Prone	81.7 ± 11.7	70.6 ± 11.1	33.66 ± 0.37	58.4 ± 9.3	48.0 ± 7.9	53.6 ± 9.4	50.5 ± 7.3	51.2 ± 7.7	50.9 ± 8.3	61.8 ± 9.0	58.1 ± 9.7
Stim-1	80.4 ± 7.3	69.7 ± 9.9	33.61 ± 0.19	60.8 ± 10.1	47.3 ± 5.8	52.6 ± 9.2	53.3 ± 7.5	54.4 ± 7.7	52.2 ± 7.3	60.3 ± 9.2	58.6 ± 8.7
Stim-2	81.7 ± 11.4	66.9† ± 10.3	33.74 ± 0.28	60.3 ± 9.7	47.9 ± 7.1	54.7 ± 9.5	54.6 ± 8.3	57.6 ± 8.9*†	57.0 ± 9.4*	62.0 ± 7.8	60.6 ± 8.8

Values are expressed as mean ± S.D. MABP: mean arterial blood pressure. *$p < 0.05$ vs. supine condition, †$p < 0.05$ vs. prone condition.

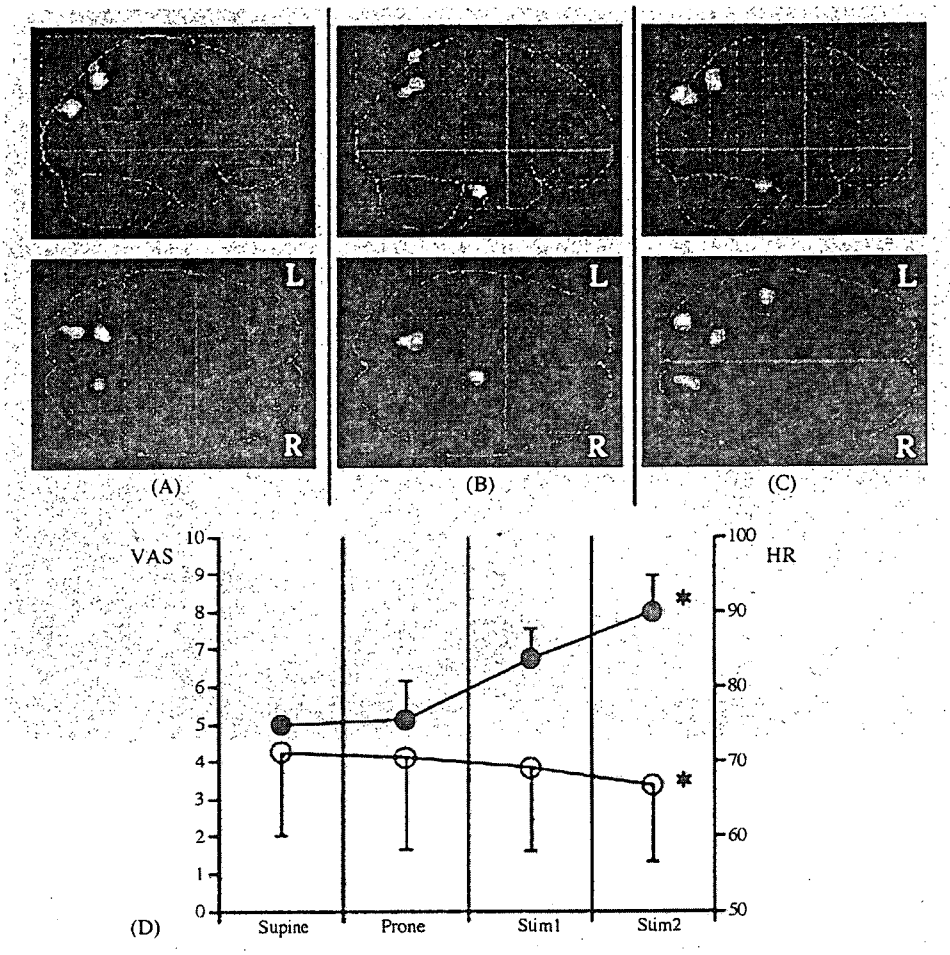

Fig. 1. Brain regions significantly activated during the prone condition vs. the supine condition (A), during the Stim-1 vs. the prone condition (B), and during the Stim-2 vs. the prone condition (C). (D) Changes in visual analog scale (VAS, ●) for relaxation and heart rate (HR, ○).

and 5.4 ± 3.4 μg/dl, respectively) than before (1.2 ± 1.7 and 6.4 ± 3.8 μg/dl, respectively), suggesting reduction in mental stress. This speculation was consistent with the finding that the VAS score for positive affect was much higher after the Stim-2 condition (Fig. 1D).

Repeated measures ANOVA showed significant increase in absolute rCBF in the parietal and occipital cortices during the Stim-2 condition compared with rCBF in the supine condition (Table 1). The parietal rCBF was also significantly higher in the Stim-2 condition than that in the prone condition. There was a tendency of rCBF elevation after assuming of prone posture in comparison with the supine posture in general.

Examination of relative increase in rCBF in the brain using voxel-based subtraction analysis in SPM2 revealed a significant elevation in rCBF in the precuneus bilaterally during the prone condition versus the supine condition (Talairach coordinates: $xyz = -18\ -62\ 50$, $Z = 5.1$; $16\ -64\ 58$, $Z = 4.6$) (Fig. 1A). Comparison of the Stim-1 condition with the prone condition showed significant increase in rCBF in the left precuneus and pons ($8\ -18\ -28$, $Z = 4.6$) (Fig. 1B). Compared with the prone condition, significant rCBF increase was found in the bilateral precuneus and left fusiform gyrus ($xyz = -46\ -28\ -24$, $Z = 4.7$) during the Stim-2 condition (Fig. 1C), in which the VAS and heart rate were significantly elevated (Fig. 1D). Correlation analysis showed a significant positive correlation of heart rate reduction with rCBF in the bilateral amygdala, orbitofrontal, hypothalamus (infundibulum) and cerebellar vermis (Fig. 2).

The present study was the first to measure rCBF quantitatively in the prone posture under palm-pressure massage applied to the back. Because each participant was released from a restraint of prone posture and allowed to sit just after each PET scan, there was less chance of a protracted prone-posture effect itself. We found that prolonged palm-pressure stimulation activated the precuneus and fusiform, along with a greater increase in parasympathetic activity and comfortable valence under the conscious state of mind. Thus, the present therapeutic maneuver may operate on the parieto-occipital region and stimulate the parasympathetic system. The present activation was in accordance with a previous report that the medial occipital cortex and lower parietal cortex were activated by relief-inducing electroacupuncture possibly through somatic-visceral sensory stimulation [24]. In addition, no increase in absolute rCBF in the frontal cortex during the present back stimulation was in line with the result from a previous PET study on hypnotics showing that the hypnotic condition caused rCBF reduction in the frontal lobe [9]. Thus, generation of comfortable sensation by the back massage may be related to rCBF increase in the posterior brain region, specifically the precuneus.

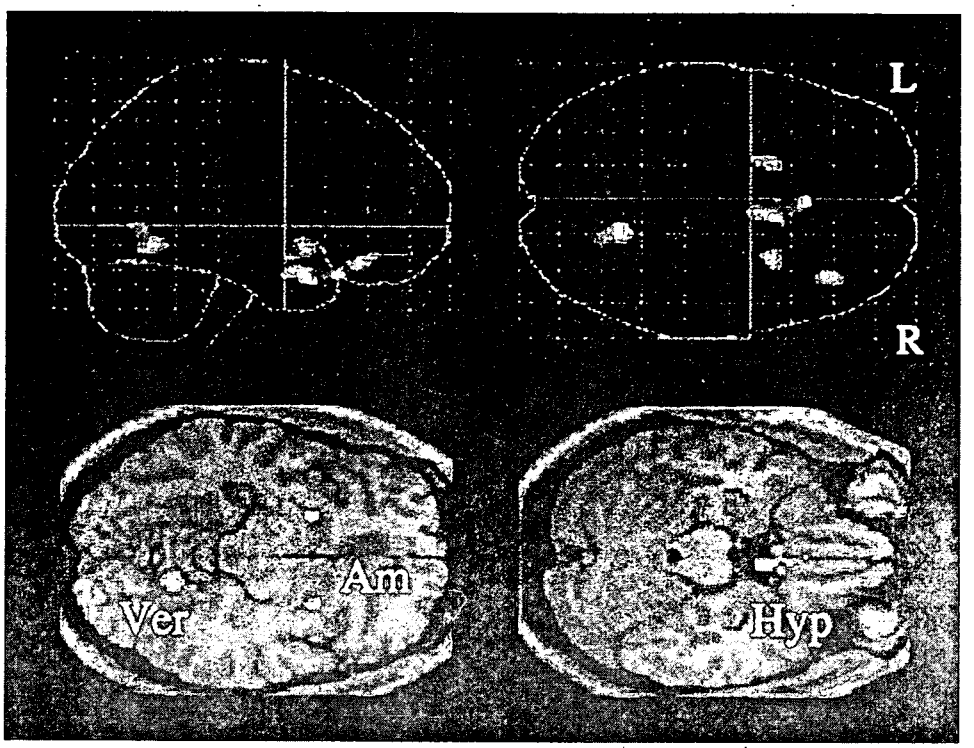

Fig. 2. Brain regions significantly correlated with reduction in heart rate. Am, amygdala; Ver, cerebellar vermis; Hyp, hypothalamus (infundibulum).

The reason for rCBF increase in the posterior brain region remains yet to be explored, but there are pieces of evidence to be noted. Regional CBF in the occipital lobe increases in a state of reduction in vigilance in parallel with the slow wave activity on electroencephalogram [19]. Visually-induced grief generates an activation of the inferior temporal and fusiform gyri [5]. The precuneus is involved in the integration of the neural network for self-consciousness, engaged in self-related mental representation [1]. In contrast, deactivation of the precuneus may indicate a loss of higher-order body or self-representation [12]. Thus, the precuneus is considered again, to play an important role in the internal mentation processes of awareness [1]. In other word, the activation of the precuneus by the back massage may reflect an augmentation of arousal and consciousness functions for positive affect.

The present VAS and neurohormonal findings verified the efficacy of the present back stimulation to reduce mental stress or anxiety in an objective sense. Before interpreting the current back massage effect, though, the methodological limitations have to be recognized because we did not apply any different types of massage that would induce mental relaxation and because we did not perform polysomnography to rule out a contamination form an early stage of sleep. However, the previous report about this massage and prompt volitional reactions just after each PET measurement (no one fell into sleep) would support the occurrence of palm-pressure effect on the neuronal and cognitive basis. In the voxel-wise correlation analysis, the bilateral amygdala, basal forebrain and cerebellar vermis were associated with reduction in heart rate. Because a PET study on biofeedback relaxation effect indicated that the region close to the hypothalamus-amygdala system serves in reducing the sympathetic bodily responses to stress and anxiety [3], the current back stimulation might affect this forebrain-amygdala system into augmenting the parasympathetic tone in the brain. The significant correlation in the cerebellum likely implies cerebellar contribution to regulating the parasympathetic system because the cerebellum is reciprocally connected to the hypothalamus, enabling to engage in the neural circuit governing autonomic function [21].

In conclusion, a prone-posture itself raises absolute rCBF in the awareness-related posterior brain region, and this rCBF increase was in association with relaxed feeling induced by back massage. The present result provided scientific evidence on its efficacy of palm-pressure massage to generate mental relaxation possibly by modulating neuronal activities in the forebrain-amygdala and precuneus network because happiness affect might be associated with the activation of the amygdala and posterior part of the cingulate cortex such as the precuneus [6].

Acknowledgments

The authors would like to thank Mr. Kenji Suzuki, Mrs. Dari Terashima, Hitomi Kimura (Balance Therapy University), Mr. Yutaka Naito (Nippon Environment Research KK), and the staff of the Positron Medical Center (Hamamatsu Medical Center) for their technical support. This study was supported by research grant from the Ministry of Health, Labor, and Welfare, Tokyo.

References

[1] A.E. Cavanna, M.R. Trimble, The precuneus: a review of its functional anatomy and behavioural correlates, Brain 129 (2006) 564–583.

[2] Z.H. Cho, S.C. Chung, J.P. Jones, J.B. Park, H.J. Park, H.J. Lee, E.K. Wong, B.I. Min, New findings of the correlation between acupoints and corresponding brain cortices using functional MRI, Proc. Natl. Acad. Sci. U.S.A. 95 (1998) 2670–2673.
[3] H.D. Critchley, R.N. Melmed, E. Featherstone, C.J. Mathias, R.J. Dolan, Brain activity during biofeedback relaxation: a functional neuroimaging investigation, Brain 124 (2001) 1003–1012.
[4] M.A. Diego, T. Field, C. Sanders, M. Hernandez-Reif, Massage therapy of moderate and light pressure and vibrator effects on EEG and heart rate, Int. J. Neurosci. 114 (2004) 31–44.
[5] H. Gundel, M.F. O'Connor, L. Littrell, C. Fort, R.D. Lane, Functional neuroanatomy of grief: an FMRI study, Am. J. Psychiatry 160 (2003) 1946–1953.
[6] U. Habel, M. Klein, T. Kellermann, N.J. Shah, F. Schneider, Same or different? Neural correlates of happy and sad mood in healthy males, Neuroimage 26 (2005) 206–214.
[7] P. Herscovitch, J. Markham, M.E. Raichle, Brain blood flow measured with intravenous H215O. I. Theory and error analysis, J. Nucl. Med. 24 (1983) 782–789.
[8] G. Ironson, T. Field, F. Scafidi, M. Hashimoto, M. Kumar, A. Kumar, A. Price, A. Goncalves, I. Burman, C. Tetenman, R. Patarca, M.A. Fletcher, Massage therapy is associated with enhancement of the immune system's cytotoxic capacity, Int. J. Neurosci. 84 (1996) 205–217.
[9] N. Kajimura, M. Nishikawa, M. Uchiyama, M. Kato, T. Watanabe, T. Nakajima, T. Hori, T. Nakabayashi, M. Sekimoto, K. Ogawa, H. Takano, E. Imabayashi, M. Hiroki, T. Onishi, T. Uema, Y. Takayama, H. Matsuda, M. Okawa, K. Takahashi, Deactivation by benzodiazepine of the basal forebrain and amygdala in normal humans during sleep: a placebo-controlled [^{15}O]H_2O PET study, Am. J. Psychiatry 161 (2004) 748–751.
[10] T. Kanno, N. Asada, H. Yanase, T. Iwanaga, T. Ozaki, Y. Nishikawa, K. Iguchi, T. Mochizuki, M. Hoshino, N. Yanaihara, Salivary secretion of highly concentrated chromogranin a in response to noradrenaline and acetylcholine in isolated and perfused rat submandibular glands, Exp. Physiol. 84 (1999) 1073–1083.
[11] S.W. Lazar, G. Bush, R.L. Gollub, G.L. Fricchione, G. Khalsa, H. Benson, Functional brain mapping of the relaxation response and meditation, Neuroreport 11 (2000) 1581–1585.
[12] P. Maquet, M.E. Faymonville, C. Degueldre, G. Delfiore, G. Franck, A. Luxen, M. Lamy, Functional neuroanatomy of hypnotic state, Biol. Psychiatry 45 (1999) 327–333.
[13] V. Napadow, N. Makris, J. Liu, N.W. Kettner, K.K. Kwong, K.K. Hui, Effects of electroacupuncture versus manual acupuncture on the human brain as measured by fMRI, Hum. Brain Mapp. 24 (2005) 193–205.
[14] A. Newberg, A. Alavi, M. Baime, M. Pourdehnad, J. Santanna, E. d'Aquili, The measurement of regional cerebral blood flow during the complex cognitive task of meditation: a preliminary SPECT study, Psychiatry Res. 106 (2001) 113–122.
[15] V. Ng, D. Koh, B.Y. Mok, S.E. Chia, L.P. Lim, Salivary biomarkers associated with academic assessment stress among dental undergraduates, J. Dent. Educ. 67 (2003) 1091–1094.
[16] Y. Ouchi, T. Kanno, E. Yoshikawa, T. Ogusu, H. Okada, K. Minoda, H. Doi, Neural correlates of muscle relaxation stimulation in the human brain, Neurosci. Res. 52 (2005) S119.
[17] Y. Ouchi, H. Okada, E. Yoshikawa, M. Futatsubashi, S. Nobezawa, Absolute changes in regional cerebral blood flow in association with upright posture in humans: an orthostatic PET study, J. Nucl. Med. 42 (2001) 707–712.
[18] O.Y. Oumeish, The cultural and philosophical aspects of pressure, massage, and touch healing as alternative therapies, Skinmed 4 (2005) 93–100.
[19] T. Paus, R.J. Zatorre, N. Hofle, Z. Caramanos, J. Gotman, M. Petrides, A.C. Evans, Time-related changes in neural systems underlyiing attention and arousal during the performance of an audiroty vigilance task, J. Cogn. Neurosci. 9 (1997) 392–408.
[20] M.D. Sauro, R.S. Jorgensen, C.T. Pedlow, Stress, glucocorticoids, and memory: a meta-analytic review, Stress 6 (2003) 235–245.
[21] J.D. Schmahmann, D. Caplan, Cognition, emotion and the cerebellum, Brain 129 (2006) 290–292.
[22] S. Wikstrom, T. Gunnarsson, C. Nordin, Tactile stimulus and neurohormonal response: a pilot study, Int. J. Neurosci. 113 (2003) 787–793.
[23] D.L. Woods, M. Dimond, The effect of therapeutic touch on agitated behavior and cortisol in persons with Alzheimer's disease, Biol. Res. Nurs. 4 (2002) 104–114.
[24] M.T. Wu, J.M. Sheen, K.H. Chuang, P. Yang, S.L. Chin, C.Y. Tsai, C.J. Chen, J.R. Liao, P.H. Lai, K.A. Chu, H.B. Pan, C.F. Yang, Neuronal specificity of acupuncture response: a fMRI study with electroacupuncture, Neuroimage 16 (2002) 1028–1037.

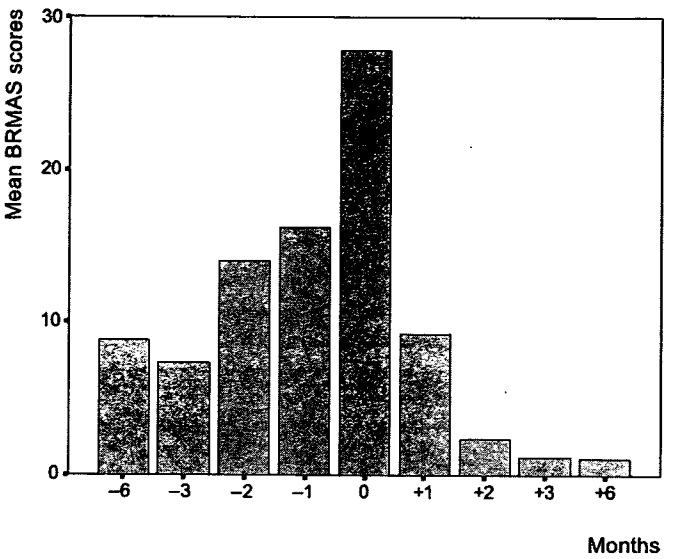

FIGURE 1. Mean BRMAS scores in patient with bipolar disorder.

significantly different between the 2 treatment periods ($P = 0.002$).

Long-acting risperidone was well tolerated. Somatic complaints were limited, with 8% dizziness and 16% constipation. No significant adverse events (including extrapyramidal symptoms) occurred.

DISCUSSION

Oral risperidone received approval from the US Food and Drug Administration for use in bipolar disorder include monotherapy for the short-term treatment of acute manic or mixed episodes associated with bipolar I disorder and combination therapy with lithium or valproate for the short-term treatment of acute manic or mixed episodes associated with bipolar disorder. A number of controlled and open-label treatment trials have demonstrated the efficacy and tolerability of risperidone in the manic phase of bipolar disorder. Risperidone has also been reported to be useful in the longer term treatment of bipolar disorder.[9]

The use of long-acting antipsychotic preparations can help to ensure compliance with therapy and has been shown to improve efficacy in relapse prevention when compared with oral agents in schizophrenia.[10]

Long-acting risperidone was associated with significant symptom improvement in patients with schizoaffective disorder,[11] but no specific mood symptom scales were used in this study. However, to our knowledge, any article related with treatment of bipolar disorder with LAR has not been published yet.

· Long-acting risperidone significantly reduced the severity of symptoms, and no manic or depressive episodes were seen in these previously noncompliant patients in 6-month period. Also, switching from mood stabilizers or mood stabilizers plus atypical antipsychotics to LAR, or adding on LAR, was safe and well tolerated in our population. These naturalistic, uncontrolled observations suggest the potential of LAR in the long-term management of bipolar I patients. Larger and controlled studies are needed to determine the role of LAR more clearly in treatment of bipolar disorder.

Haluk A. Savas, MD
Mehmet Yumru, MD
Murat Eren Özen, MD
Department of Psychiatry
Gaziantep University Faculty of Medicine, Gaziantep, Turkey
drmehmetyumru@yahoo.com

REFERENCES

1. Fountoulakis KN, Vieta E, Sanchez-Moreno J, et al. Treatment guidelines for bipolar disorder: a critical review. *J Affect Disord.* 2005;860:1–10.
2. Yatham LN. Efficacy of atypical antipsychotics in mood disorders. *J Clin Psychopharmacol.* 2003;23:9–14.
3. Brambilla P, Barale F, Soares JC. Atypical antipsychotics and mood stabilization in bipolar disorder. *Psychopharmacology (Berl).* 2003;166:315–332.
4. Tohen M, Ketter TA, Zarate CA, et al. Olanzapine versus divalproex sodium for the treatment of acute mania and maintenance of remission: a 47-week study. *Am J Psychiatry.* 2003;160:1263–1271.
5. Yatham LN, Binder C, Riccardelli R, et al. RIS-CAN 25 Study Group: risperidone in acute and continuation treatment of mania. *Int Clin Psychopharmacol.* 2003;18:227–235.
6. Lasser RA, Bossie CA, Gharabawi GM, et al. Remission in schizophrenia: results from a 1-year study of long-acting risperidone injection. *Schizophr Res.* 2005;77:215–227.
7. Montgomery DB. European College of Neuropsychopharmacology ECNP Consensus Meeting March 2000 Nice: guidelines for investigating efficacy in bipolar disorder. European College of Neuropsychopharmacology. *Eur Neuropsychopharmacol.* 2001;11:79–88.
8. Jensen HV, Plenge P, Mellerup ET, et al. Lithium prophylaxis of manic-depressive disorder: daily lithium dosing schedule versus every second day. *Acta Psychiatr Scand.* 1995;92:69–74.
9. Sajatovic M, Madhusoodanan S, Fuller MA, et al. Risperidone for bipolar disorders. *Expert Rev Neurother.* 2005;5:177–187.
10. Ereshefsky L, Mannaert E. Pharmacokinetic profile and clinical efficacy of long-acting risperidone: potential benefits of combining an atypical antipsychotic and a new delivery system. *Drugs R D.* 2005;6:129–137.
11. Lasser RA, Bossie CA, Gharabawi GM, et al. Efficacy and safety of long-acting risperidone in stable patients with schizoaffective disorder. *J Affect Disord.* 2004;83:263–275.

Perospirone Is a New Generation Antipsychotic

Evidence From a Positron Emission Tomography Study of Serotonin 2 and D_2 Receptor Occupancy in the Living Human Brain

To the Editors:

Since perospirone has been shown to have a high affinity for both serotonin

2 (5-HT2) and D_2 dopamine receptors in rodents, the agent has been classified among the new generation antipsychotics.[1] However, it remains unknown whether the agent has the similar pharmacological action (ie, operating on the 5-HT2 receptor as well as the D_2 dopamine receptor) in the living human brain. We therefore used positron emission tomography (PET) to investigate whether perospirone would indeed act on 5-HT2 and D_2 dopamine receptors in the in vivo brains of healthy humans, and we also evaluated the possibility of a relationship between perospirone plasma concentration and 5-HT2 receptor and D_2 dopamine receptor occupancy.

This study was approved by the local ethics committee. Written informed consent was obtained from each of the subjects. Four healthy men (mean age ± SD, 35.0 ± 3.2 years; mean body weight ± SD, 73.3 ± 4.3 kg) participated in this study. Occupancy measurements of 5-HT2 and D_2 dopamine receptors were performed on 2 separate days, at least 2 weeks apart, in the following order: 5-HT2 receptor occupancy on the first day and D_2 dopamine receptor occupancy on the second day. On each day, 2 PET scans were performed. The first PET scan was performed to determine the baseline radioligand binding level. Subsequently, perospirone was administered as 8-mg tablet 6 hours after the establishment of the baseline value. The dosage was chosen based on tolerability in healthy subjects.[2] Then, the second PET scan was performed 1 hour after the subject was given perospirone because it has been reported that in healthy humans, oral perospirone can reach the maximum plasma level at that time approximately 1 hour after administration.[2,3] [^{11}C]N-methylspiperone was used as a tracer for the determination of 5-HT2 receptor occupancy, and [^{11}C]raclopride was used to determine D_2 dopamine receptor occupancy.[4,5] To quantify 5-HT2 and D_2 dopamine occupancy, we applied an equilibrium ratio analysis that used the ratio between the total radioactivity in the region of interest (ROI) and that in a reference region with negligible density.[5,6] The frontal cortex was used as the ROI for the calculation of 5-HT2 receptor occupancy, whereas the putamen was used as the ROI for D_2 dopamine receptor occupancy. The cerebellar cortex was used as a reference region in both examinations. To minimize the contribution of the partial volume effect, magnetic resonance images were superimposed onto PET images according to previously described procedures.[7] During the scan performed after the administration of perospirone, a total of 5 blood samples were withdrawn periodically at intervals of 15 minutes after the injection of the tracer. The samples were analyzed by high-performance liquid chromatography for the determination of the perospirone plasma concentrations.[8] The mean concentration of the 5 samples was used as the representative perospirone plasma concentration during the PET scanning procedure. The preclinical observations suggest that perospirone has at least 13 nonactive and 4 active metabolites, including hydroxyperospirone, which has the highest affinity for both 5-HT2 and D_2 receptors among the known metabolites; however, even hydroxyperospirone has one eighth or even less of the affinity for both 5-HT and D_2 receptors than that of unmetabolized perospirone.[2] Therefore, in the present study, we restricted our evaluation to the relationship between the unmetabolized perospirone plasma concentration and receptor occupancy. The relationship between the perospirone plasma concentration and receptor occupancy was modeled according to the following equation: $\%Occupancy = 100 \times pConc/ (ED_{50} + pConc)$, where ED_{50} is the perospirone concentration at which 50% receptor occupancy is achieved, and pConc is the perospirone plasma concentration.[5,6,9] The severity of extrapyramidal symptoms (EPSs) was assessed using the Simpson-Angus Rating Scale for EPSs[10] and the Barnes Akathisia Rating Scale.[11]

All 4 participants completed the study. None of the participants exhibited EPSs. Each subject's paired values of 5-HT2 occupancy (perospirone concentration)/D_2 receptor occupancy (perospirone concentration) were as follows: subject 1 is equal to 39.6% (0.7 ng/mL)/36.1% (1.2 ng/mL); subject 2, 65.6% (2.4 ng/mL)/11.9% (0.5 ng/mL); subject 3, 51.4% (1.3 ng/mL)/62.7% (1.6 ng/mL); and subject 4, 68.6% (2.4 ng/mL)/67.1% (2.1 ng/mL). The mean ± SD value for 5-HT2 receptor occupancy after oral administration of 8-mg perospirone was 56.3% ± 13.4%, and that for D_2 dopamine receptor occupancy was 44.4% ± 25.7%. The modeled curves relating plasma levels and receptor occupancies were found fit well (Fig. 1). In the present study of the oral administration of an 8-mg dose of perospirone, the values of ED_{50} for 5-HT2 and D_2 receptors were 1.2 and 1.4 ng/mL, respectively.

DISCUSSION

Our results indicated that perospirone, when administered at an oral dose of 8 mg, led to the occupancy of both the 5-HT2 receptor and the D_2 receptor in the living human brain; furthermore, these 2 types of occupancy increased in accordance with increases in plasma levels of perospirone, thus suggesting that perospirone shares the pharmacological profile of the serotonin-dopamine antagonist family of agents.[12] The curves that relate dose and occupancy reveal a similar pattern between the pharmacokinetic responses to perospirone and risperidone;[13] this observation suggests that these 2 agents may share clinically similar profiles. In fact, it has been reported that perospirone is associated with not only a dose-related increase in risk of EPSs but also a dose-related rise in the plasma prolactin concentration,[3] both of which are generally observed after the administration of risperidone to humans.

It has been suggested that nearly 70% to 80% of D_2 receptor occupancy is suitable for obtaining a sufficient antipsychotic effect with a minimal risk of EPS in most patients with schizophrenia.[5] In this study, the range of plasma perospirone concentrations within which 70% to 80% occupancy of the D_2 receptor would be achieved was estimated at 3.4 to 5.8 ng/mL (see Fig. 1), suggesting that maintaining a

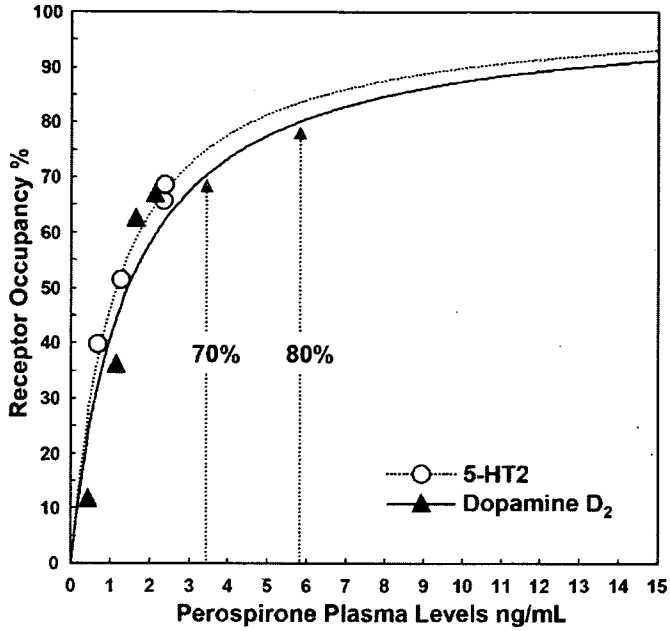

FIGURE 1. Relationship between 5-HT2 and D_2 receptor occupancy and perospirone plasma concentration levels in 4 healthy men administered an 8-mg dose of perospirone.

median level within this range, that is, an approximate perospirone plasma concentration of 4.5 ng/mL could provide an optimal initial treatment that would yield antipsychotic effects with a minimal risk of EPS. However, it should be noted that there was considerable individual variability in perospirone plasma concentration (range, 0.5–2.4 ng/mL), which is consistent with the results of previous studies.[2,3,8] In fact, the D_2 receptor occupancy varied from 11.9% to 67.1% despite the administration of identical dosage of perospirone. Studies with larger sample sizes will be needed to verify the present findings and to further explore this issue.

To the best of our knowledge, this is the first PET study to provide direct evidence in support of the notion that perospirone possesses the properties of an serotonin-dopamine antagonist in the human brain in vivo. Our findings of a relationship between perospirone plasma levels and the occupancy of 5-HT2 and D_2 receptors may offer a useful guide for determining the therapeutic dosage of perospirone with minimal side effects in patients with schizophrenia.

ACKNOWLEDGMENTS

The authors would like to thank Messrs Yoshimasa Inoue and Toshihiko Kanno for the excellent technical support.

This work was supported by a grant from The Stanley Medical Research Institute and a Grant-in-Aid for the Center of Excellence from the Ministry of Education, Culture, Sports, Science, and Technology, Japan.

Yoshimoto Sekine, MD, PhD*
Yasuomi Ouchi, MD, PhD†
Nori Takei, MD, PhD, MSc*‡
Etsuji Yoshikawa, BA§
Hiroyuki Okada, BA§
Yoshio Minabe, MD, PhD*
Kazuhiko Nakamura, MD, PhD*
Katsuaki Suzuki, MD, PhD*
Yasuhide Iwata, MD, PhD*
Kenji J. Tsuchiya, MD, PhD*
Genichi Sugihara, MD*
Norio Mori, MD, PhD*
*Department of Psychiatry and Neurology
Hamamatsu University School of Medicine
Hamamatsu, Japan
†Positron Medical Center
Hamamatsu Medical Center
Hamakita, Japan
‡Division of Psychological Medicine
Department of Psychiatry
Institute of Psychiatry, De Crespigny Park
London, UK
§Central Research Laboratory, Hamamatsu
Photonics KK Hamakita, Japan
ysekine@hama-med.ac.jp

REFERENCES

1. Onrust SV, McClellan K. Perospirone. *CNS Drugs.* 2001;15:329–337.
2. Japan Pharmacists Education Center. *New Drug Approval Package No. 61: Perospirone.* (in Japanese); 2000.
3. Yasui-Furukori N, Furukori H, Nakagami T, et al. Steady-state pharmacokinetics of a new antipsychotic agent perospirone and its active metabolite, and its relationship with prolactin response. *Ther Drug Monit.* 2004; 26:361–365.
4. Nyberg S, Farde L, Eriksson L, et al. 5-HT2 and D2 dopamine receptor occupancy in the living human brain. A PET study with risperidone. *Psychopharmacology.* 1993;110:265–272.
5. Nyberg S, Eriksson B, Oxenstierna G, et al. Suggested minimal effective dose of risperidone based on PET-measured D2 and 5-HT2A receptor occupancy in schizophrenic patients. *Am J Psychiatry.* 1999;156:869–875.
6. Farde L, Nordstrom AL, Wiesel FA, et al. Positron emission tomographic analysis of central D1 and D2 dopamine receptor occupancy in patients treated with classical neuroleptics and clozapine. Relation to extrapyramidal side effects. *Arch Gen Psychiatry.* 1992;49:538–544.
7. Sekine Y, Ouchi Y, Takei N, et al. Brain serotonin transporter density and aggression in abstinent methamphetamine abusers. *Arch Gen Psychiatry.* 2006;63:90–100.
8. Yasui-Furukori N, Inoue Y, Tateishi T. Determination of a new atypical antipsychotic agent perospirone and its metabolite in human plasma by automated column-switching high-performance liquid chromatography. *J Chromatogr B Analyt Technol Biomed Life Sci.* 2003;789:239–245.
9. Remington G, Kapur S, Zipursky R. The relationship between risperidone plasma levels and dopamine D2 occupancy: a positron emission tomographic study. *J Clin Psychopharmacol.* 1998;18:82–83.
10. Simpson GM, Angus JW. A rating scale for extrapyramidal side effects. *Acta Psychiatr Scand (Suppl).* 1970;212:11–19.
11. Barnes TR. A rating scale for drug-induced akathisia. *Br J Psychiatry.* 1989;154:672–676.
12. Meltzer HY. The role of serotonin in schizophrenia and the place of serotonin-dopamine antagonist antipsychotics. *J Clin Psychopharmacol.* 1995;15(suppl 1):2S–3S.
13. Kapur S, Zipursky RB, Remington G. Clinical and theoretical implications of 5-HT2 and D2 receptor occupancy of clozapine, risperidone, and olanzapine in schizophrenia. *Am J Psychiatry.* 1999;156:286–293.

ELSEVIER

Journal of the Neurological Sciences xx (2006) xxx–xxx

Journal of the Neurological Sciences

www.elsevier.com/locate/jns

Short communication

Dopaminergic neuronal dysfunction associated with parkinsonism in both a Gaucher disease patient and a carrier

Satoshi Kono [a,*], Kentaro Shirakawa [a], Yasuomi Ouchi [b], Masanobu Sakamoto [b], Hiroyuki Ida [c], Takeshi Sugiura [a], Hiroyuki Tomiyama [d], Hitoshi Suzuki [a], Yoshitomo Takahashi [a], Hiroaki Miyajima [a], Nobutaka Hattori [d], Yoshikuni Mizuno [d]

[a] *First Department of Medicine, Hamamatsu University School of Medicine, 1-20-1 Handayama, Hamamatsu 431-3192, Japan*
[b] *Department of Neurology, Positron Medical Center, Hamamatsu Medical Center, Hamamatsu, Japan*
[c] *Department of Pediatrics, Jikei University School of Medicine, Tokyo, Japan*
[d] *Department of Neurology, Juntendo University School of Medicine, Tokyo, Japan*

Received 8 September 2006; received in revised form 23 October 2006; accepted 30 October 2006

Abstract

A clinical association between Gaucher disease and parkinsonism has been demonstrated. We herein report a Japanese patient with type 3 Gaucher disease who was compound heterozygous for F213I and L444P mutations in the glucocerebrosidase gene while his father was heterozygous for the L444P mutation. They both presented with parkinsonism characterized by a predominance of akinetic-rigid signs and a favorable response to anti-Parkinson therapies. We investigated the dopaminergic neuronal function using positron emission tomography (PET) with radioligands, [^{11}C] CFT and [^{11}C] raclopride. PET studies of both patients demonstrated the [^{11}C] CFT uptake to be severely decreased in the putamen and the caudate nucleus, however, the [^{11}C] raclopride uptake was normal in the basal ganglia. Although the majority of Gaucher disease patients with parkinsonism tend to be refractory to anti-Parkinson therapies. The clinical features and the findings of the PET studies suggest that patients with parkinsonism associated with the mutation in the glucocerebrosidase gene, even in heterozygosis, may be related to the presynaptic dopaminergic neuronal dysfunction reported in Parkinson's disease. A PET study to evaluate the dopaminergic neuronal function in Gaucher disease would provide both a better understanding of the effects of anti-Parkinson therapies and a help to improve our ability to make an early diagnosis of parkinsonism associated with Gaucher disease.

Keywords: Gaucher disease; Parkinsonism; Glucocerebrosidase; PET

1. Introduction

Gaucher disease is an autosomal recessive lysosomal disorder resulting from a deficiency of the lysosomal enzyme glucocerebrosidase which lead to the systemic storage of glycosphingolipids [1]. This disease is caused by mutations in the glucocerebrosidase gene located on1q21. Recent studies have revealed an association between Gaucher disease and Parkinson's disease due to a concurrence of type 1 Gaucher disease and parkinsonism and the identification of glucocerebrosidase mutations in patients with sporadic Parkinson's disease [2–7]. Initial studies of the patients affected from Gaucher disease with the parkinsonism showed that the parkinsonism was characterized by an early onset and it tended to be refractory to levodopa therapy [2,3,5], however, there is an increasing number of reports which showed parkinsonism to demonstrate the following signs of typical Parkinson disease: namely, the asymmetric onset of rigidity, resting tremor, bradykinesia, and a favorable response to Parkinson therapies [4,8]. Treatment-refractory parkinsonism suggests that mutations in the glucocerebrosidase gene may affect either postsynaptic dopaminergic neurons or both post- and presynaptic dopaminergic neurons.

* Corresponding author. Tel.: +81 53 435 2261; fax: +81 53 434 9447.
E-mail address: satokono@hama-med.ac.jp (S. Kono).

0022-510X/$ - see front matter © 2006 Elsevier B.V. All rights reserved.
doi:10.1016/j.jns.2006.10.019

Please cite this article as: Kono S et al. Dopaminergic neuronal dysfunction associated with parkinsonism in both a Gaucher disease patient and a carrier. J. Neurol. Sci. (2006), doi:10.1016/j.jns.2006.10.019

We herein investigated the dopaminergic neuronal function of the parkinsonism, responsive to levodopa therapy, in a type 3 Gaucher disease patient and his father using positron emission tomography (PET) and thus showed that our cases were involved in presynaptic dopaminergic function seen in Parkinson's disease.

2. Clinical reports

A 38-year-old Japanese man complained of difficulty in walking and a reduced speed in the normal activities of daily life. He was found to have hepatosplenomegaly at the age 6. A bone marrow analysis revealed a marked accumulation of Gaucher's cells and his glucocerebrosidase activity level was 1.8 nmol/h/mg protein (control level; 4.1–9.6 nmol/h/mg protein). He developed a generalized tonic–clonic seizure with abnormal electroencephalogram patterns at age 7 and thus was treated with anti-convulsant therapy. A neurological examination at the age 7 slowed horizontal saccadic eye movements characteristic of type 3 Gaucher disease. He was diagnosed to have type 3 Gaucher disease and thus underwent a splenectomy in early adolescence. He also suffered from spinal bone pain and abdominal pain associated with hepatomegaly at the age 28. After the initiation of enzyme replacement therapy at the age 33, the hepatomegaly and the bone pain both were improved, however, the patient gradually developed a clumsy left hand, start hesitation and freezing of gait during turning. He was unable to walk without assistance by the age 37 and thereafter presented at our hospital. His family history revealed no consanguinity and no history of Gaucher disease. A neurological examination revealed that he showed severe akinesia with a tendency to show trunk deviation to the left in the sitting position and he was unable to get up from a chair without help. He walked with a flexed posture, with small and irregular steps, while demonstrating start and turn hesitation and a reduction in his arm swing. Slurred speech, hypophonia, micrographia and generalized rigidity were also observed, as well as slowed horizontal saccadic eye movements. All other neurological examinations were unremarkable; in particular involuntary movement including tremors, and muscle strength, stretch and cutaneous plantar reflexes, co-ordination, sensory functions, or fundi and other cranial nerves were normal. A mental examination showed him to be inert. Spatial abilities were intact. His digit span was six forward, and four backward. He could repeat a seven-item name and address immediately after its oral presentation and could recall 6 of 7 items after a 5-minute delay. The Wechsler Adult Intelligence Scale (WAIS) showed verbal IQ of 60, performance IQ of 53, and full scale IQ of 52His Mini Mental State Examination (MMSE) score was 26. An electroencephalogram showed some sharp waves or spike and wave complexes over both parietal-occipital regions and abundant generalized discharges of spikes, polyspikes and slow wave complexes. Magnetic resonance imaging showed no abnormality in the brain. A slit-lamp examination and laboratory studies including thyroid function tests, serum copper and ceruloplasmin were all normal. The study of an auditory brainstem response in this patient showed no deterioration.

His 71-year-old father presented to our hospital in order to help his son. He also became aware of progressive difficulty of slowness during walking and developed a left clumsy hand at the age of 63. A neurological examination showed bradykinesia, symmetrical cogwheel rigidity of the upper limbs and poor backward postural reflexes. His sense of touch, vibration, position and cognitive abilities were intact. Her 65-year-old mother was asymptomatic. A neurological examination was unremarkable.

After PET studies of the proband and his farther, anti-Parkinson therapies including levodopa/carbidopa, cabergoline and selegeline HCl were initiated. The parkinsonian features in both patients showed a favorable response to the medication. The patient was able to walk without assistance and showed an improvement in both akinesia and rigidity. The Unified Parkinson disease rating scale (UPDRS) III motor score in the proband improved from 45 to 28. His father also improved from 23 to 16. During the follow-up, the proband showed a gradual appearance of a wearing-off phenomenon, motor fluctuations and levodopa-induced dyskinesia.

3. Methods and results

3.1. Molecular genetic analysis

Genomic DNA samples isolated from blood samples were subjected to restriction fragment length polymorphism (RFLP) analyses to identify any mutations in the glucocerebrosidase gene by a previous described method [9] For a molecular genetic analysis for hereditary Parkinson disease, the sequencing of the gene for α-synuclein and parkin was performed by a previously reported technique [10,11]. The genetic study demonstrated that the proband carried two known missence mutations in the glucocerebrosidase gene, L444P in exon 10 and F213I in exon 6 (Fig. 1A). The RFLP analyses of his father demonstrated a L444P mutation on the paternal allele. No mutations in the α-synuclein gene or the parkin gene were identified in the proband and his father.

3.2. PET scan

PET was performed by a high-resolution brain PET scanner (SHR12000, Hamamatsu Photonics K.K., Hamamatsu, Japan). The head of a patient was fixated using a thermoplastic face-mask enabling to fix it to the same place between separate PET measurements. First, 72 min after a bolus intravenous injection of the [^{11}C] CFT, 20-minute PET data were collected to produce a late-phase image of [^{11}C] CFT uptake [12]. Next, following three hours to allow for a decay of [^{11}C] CFT radioactivity, the same patient were scanned for 62 min after [^{11}C] raclopride injection using a

Please cite this article as: Kono S et al. Dopaminergic neuronal dysfunction associated with parkinsonism in both a Gaucher disease patient and a carrier. J. Neurol. Sci. (2006), doi:10.1016/j.jns.2006.10.019

serial scans protocol [13] The final PET images were generated as semi-quantitative parametric images (a standardized uptake value image for [^{11}C] CFT, and a distribution image for [^{11}C] raclopride). Based on the regions of interest (ROIs) method, we placed the ROIs on the caudate nucleus, putamen and cerebellum on the MR images, and then transferred them onto the corresponding PET images, and finally calculated a semi-quantitative striatum/cerebellum ratio by dividing the ROI counts of either the caudate nucleus or the putamen by cerebellar counterparts. The ratio from a patient and his father was compared with the ratios from three normal control subjects and assessed statistically by one sample t-test (Table 1). The PET images of the patient and his father showed similar results. The uptake of [^{11}C] CFT in the both putamen and caudate nucleus was significantly reduced ($p<0.05$), while the [^{11}C] raclopride uptake showed a relative decrease in the same striatal regions in comparison with normal counterparts.

Table 1

	Patient	His father	Normal subjects (n=3) (mean±S.D.)
[^{11}C] CFT			
Caudate nucleus/cerebellum ratio	1.82	1.56	3.83±0.07
Putamen/cerebellum ratio	1.42	1.37	3.90±0.13
[^{11}C] raclopride			
Caudate nucleus/cerebellum ratio	3.93	3.72	4.33±0.13
Putamen/cerebellum ratio	4.02	4.14	4.49±0.31

The uptake of [^{11}C] CFT in the both putamen and caudate nucleus was significantly reduced at $p<0.05$ by one sample t-test.

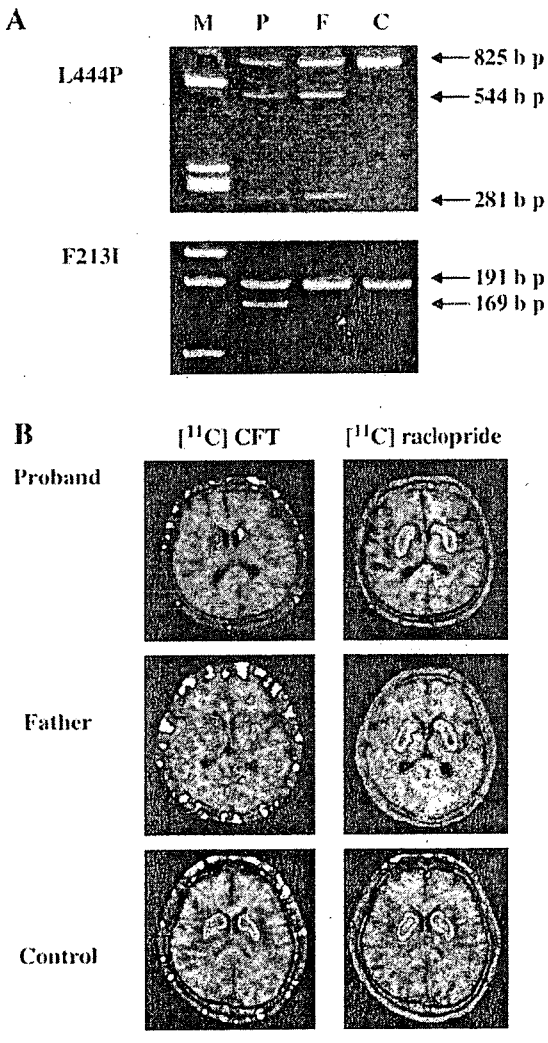

Fig. 1. A. Restriction fragment length polymorphism analyses of the L444P and the F213I mutation in the patient and his father. When the L444P mutation is present, restriction enzyme (NciI) digests an 825 bp PCR product, thus producing two fragments of 544 bp and 281 bp. When the F213I mutation is present, a restriction enzyme (AseI) digests a 191 bp PCR thereby producing two fragments of 169 bp and 22 bp M: molecular marker, P: patient, F: patient's father, C: control. B. Transaxial PET slices blended with MRI images of the proband, his father and a 38-year-old healthy man as a control.

4. Discussion

This report documented fascinating clinical and PET findings in two patients with the same family lineage who both developed parkinsonism. The clinical features of our cases are as follows; 1) the proband with type 3 Gaucher disease and his father developed parkinsonism, 2) molecular genetic analyses in the glucocerebrosidase gene showed the proband to be compound heterozygous for L444P and F213I, while his father is heterozygous for the L444P mutation, 3) the parkinsonism showed a favorable response to anti-Parkinson therapies and 4) a dopaminergic functional neuroimaging study of both patients showed a presynaptic dopaminergic dysfunction which is normally seen in Parkinson's disease patients. Parkinsonism has been described as a rare neurological phenotype of patients with type 1 Gaucher disease [2,3] The parkinsonism in such patients is characteristically early-onset and most tend to show a poor response to levodopa therapy. The enzyme replacement therapy is not effective for the treatment of the parkinsonism in such cases. The neuropathological findings characteristic to Gaucher disease with parkinsonism showed a marked loss of dopaminergic neurons in the substantia nigra, synuclein-positive Lewy bodies and the involvement of hippocampal CA2-4 regions where glucocerebrosidase was expressed [5,14]. While the concurrence of Gaucher disease and parkinsonism could still be coincidental, the shared clinical characteristics and neuropathology of previous case reports suggest a related etiology. In our proband the diagnosis of Gaucher disease was firmly established both by a deficiency in the glucocerebrosidase activity and the gene analysis in the glucocerebrosidase gene. The first clinical manifestations including hepatosplenomegaly, slow saccadic eye movements and epilepsy preceded by osseous pain, appearing in adulthood, suggest our case to have type 3 Gaucher disease The L444P and the F213I mutations identified in our patients

Please cite this article as: Kono S et al. Dopaminergic neuronal dysfunction associated with parkinsonism in both a Gaucher disease patient and a carrier. J. Neurol. Sci. (2006), doi:10.1016/j.jns.2006.10.019

are frequent in patients affected with both type 1 and 2 as well as type 3 Gaucher disease [1,9]. Although the correlation between genotypes and phenotypes in Gaucher disease is investigated, the conclusion remains elusive [1] Although many reports have demonstrated a clinical association between type 1 Gaucher disease and parkinsonism, type 3 Gaucher disease with parkinsonism is uncommon. The proband appeared to have early-onset parkinsonism which developed in his 30's as previous reports in type 1 Gaucher disease patients with parkinsonism [5]. The patient's father who carried the L444P allele developed parkinsonism in his 60's. A recent study demonstrates that parkinsonism appears to be associated with heterozygosity for a mutation in the glucocerebrosidase gene [8]. This observation indicates that the L444P mutation found in the father, even in heterozygotes, may thus be a risk factor for the development of parkinsonism. The correlation between parkinsonism as a phenotype and mutations in the glucocerebrosidase gene as a genotype has not yet been established. N370S, L444P, 84GG mutations are reported as common mutations associated with parkinsonism in Gaucher disease patients and their carriers, however, it is evident that the majority of the patients or carriers with such mutations do not always develop parkinsonism [4,5,8] An intriguing clinical feature of our patients was the fact that they had treatment-responsive parkinsonism, because initial case reports showed the parkinsonian symptoms in Gaucher disease patients to be refractory to levodopa therapy [2,3,5]. In addition, the association between a favorable response to L-Dopa and the mutation in patients with Gaucher disease has been reported in some studies. Bembi et al. reported 4 cases with a good response to L-Dopa who had either N370S, L444P or G337S mutation [4]. Goker-Alpan et al. also showed some cases with a good response to L-Dopa therapy and they had either N370S or L444P mutations, however, not all the patients with such a mutation always showed an effective response to L-Dopa therapy [8].

We evaluated the dopaminergic function of our patients using neuroimaging techniques with a PET system [^{11}C] CFT, a dopamine transporter probe, allows us to study the integrity of the presynaptic dopaminergic system [12]. [^{11}C] raclopride, a low affinity dopaminergic D2 receptor ligand, has been used to study the post synaptic dopaminergic function [13]. The PET study with the combined use of [^{11}C] CFT and [^{11}C] raclopride in our patients who both carried the L444P mutation allele showed a presynaptic dopaminergic dysfunction The mutation in the glucocerebrosidase gene, even in heterozygosis, may be associated with the presynaptic dopaminergic neuronal dysfunction which shares a common pathogenesis to Parkinson's disease. It is not clear why the parkinsonism associated with mutations in the glucocerebrosidase gene shows such variation in the responsiveness to levodopa therapy. We speculate that at the onset of the parkinsonism, this mutation may be associated with a dysfunction of presynaptic dopaminergic neuron and then, during the progression of the parkinsonism, the patient may develop dysfunction of postsynaptic dopaminergic neurons resulting in the poor responsiveness to levodopa therapy. Another possibility may be that other genetic or environmental factors may interact with the glucocerebrosidase gene thus resulting in the development of variation in the responsiveness to anti-Parkinson therapy. It is important to be aware of the association between Gaucher disease and parkinsonism. We should therefore investigate parkinsonian symptoms in not only probands of Gaucher disease but also their family members. A PET study to evaluate pre- and postsynaptic dopaminergic neuronal function provides an excellent understanding of an association with Gaucher disease and Parkinson's disease.

References

[1] Sidransky E. Gaucher disease: complexity in a "simple" disorder. Mol Genet Metab 2004;83:6–15.

[2] Neudorfer O, Giladi N, Elstein D, Abrahamov A, Turezkite T, Aghai E, et al. Occurrence of Parkinson's syndrome in type I Gaucher disease. QJM 1996;89:691–4.

[3] Varkonyi J, Simon Z, Soos K, Poros A. Gaucher disease type I complicated with Parkinson's syndrome. Haematologia (Budap) 2002;32:271–5.

[4] Bembi B, Zambito Marsala S, Sidransky E, Ciana G, Carrozzi M, Zorzon M, et al. Gaucher's disease with Parkinson's disease: clinical and pathological aspects. Neurology 2003;61:99–101.

[5] Tayebi N, Walker J, Stubblefield B, Orvisky E, LaMarca ME, Wong K, et al. Gaucher disease with parkinsonian manifestations: does glucocerebrosidase deficiency contribute to a vulnerability to parkinsonism? Mol Genet Metab 2003;79:104–9.

[6] Aharon-Peretz J, Rosenbaum H, Gershoni-Baruch R. Mutations in the glucocerebrosidase gene and Parkinson's disease in Ashkenazi Jews. N Engl J Med 2004;351:1972–7.

[7] Zimran A, Neudorfer O, Elstein D. The glucocerebrosidase gene and Parkinson's disease in Ashkenazi Jews. N Engl J Med 2005;352:728–31 [author reply 728-31].

[8] Goker-Alpan O, Schiffmann R, LaMarca ME, Nussbaum RL, McInerney-Leo A, Sidransky E. Parkinsonism among Gaucher disease carriers. J Med Genet 2004;41:937–40.

[9] Ida H, Rennert OM, Kawame H, Ito T, Maekawa K, Eto Y. Mutation screening of 17 Japanese patients with neuropathic Gaucher disease. Hum Genet 1996;98:167–71.

[10] Kitada T, Asakawa S, Hattori N, Matsumine H, Yamamura Y, Minoshima S, et al. Mutations in the parkin gene cause autosomal recessive juvenile parkinsonism. Nature 1998;392:605–8.

[11] Chan P, Jiang X, Forno LS, Di Monte DA, Tanner CM, Langston JW. Absence of mutations in the coding region of the alpha-synuclein gene in pathologically proven Parkinson's disease. Neurology 1998;50:1136–7.

[12] Ouchi Y, Kanno T, Okada H, Yoshikawa E, Futatsubashi M, Nobezawa S, et al. Changes in dopamine availability in the nigrostriatal and mesocortical dopaminergic systems by gait in Parkinson's disease. Brain 2001;124:784–92.

[13] Ouchi Y, Yoshikawa E, Futatsubashi M, Okada H, Torizuka T, Sakamoto M. Effect of simple motor performance on regional dopamine release in the striatum in Parkinson disease patients and healthy subjects: a positron emission tomography study. J Cereb Blood Flow Metab 2002;22:746–52.

[14] Wong K, Sidransky E, Verma A, Mixon T, Sandberg GD, Wakefield LK, et al. Neuropathology provides clues to the pathophysiology of Gaucher disease. Mol Genet Metab 2004;82:192–207.

Please cite this article as: Kono S et al. Dopaminergic neuronal dysfunction associated with parkinsonism in both a Gaucher disease patient and a carrier. J. Neurol. Sci. (2006), doi:10.1016/j.jns.2006.10.019

Journal of Cerebral Blood Flow & Metabolism (2006), 1–8

www.jcbfm.com

In vivo presynaptic and postsynaptic striatal dopamine functions in idiopathic normal pressure hydrocephalus

Yasuomi Ouchi[1], Teiji Nakayama[2], Toshihiko Kanno[1], Etsuji Yoshikawa[3], Tomomi Shinke[3] and Tatsuo Torizuka[1]

[1]*Positron Medical Center, Hamamatsu Medical Center, Hamamatsu, Japan;* [2]*Department of neurosurgery, Hamamatsu Medical Center, Hamamatsu, Japan;* [3]*Central Research Laboratory, Hamamatsu Photonics KK, Hamamatsu, Japan*

Differentiation of impaired gait seen in idiopathic normal pressure hydrocephalus (iNPH) from parkinsonian gait is sometimes a great challenge and important for future medication in the clinical setting. To investigate dopaminergic contribution to its pathophysiology, two aspects of the transsynaptic dopamine functions in the striatal region in eight iNPH patients naïve to dopaminergic drugs were examined using positron emission tomography with a presynaptic marker [^{11}C]CFT ([^{11}C]2-β-carbomethoxy-3β-(4-fluorophenyl) tropane) that binds to dopamine transporter and a postsynaptic marker [^{11}C]raclopride that binds to D2 receptor. Quantitative values of binding potentials (BPs) for [^{11}C]CFT and [^{11}C]raclopride were compared between patients and eight age-matched healthy subjects. The BPs and magnetic resonance imaging-based morphometric measures in iNPH were used for correlation analyses between the magnitude of binding of these *in vivo* markers and clinical severity of the patients. Analysis of variance showed significant reduction in [^{11}C]raclopride binding in the putamen and nucleus accumbens ($P<0.05$, corrected for multiple comparison) and unchanged striatal [^{11}C]CFT binding in iNPH. The dorsal putamen [^{11}C]raclopride binding correlated negatively with gait severity ($r=0.720$, $P<0.05$), and the nucleus accumbens [^{11}C]raclopride binding correlated positively with emotional recognition score ($r=0.727$, $P<0.05$) in the disease group. No significant relationship was observed between BPs and morphometric measures. The current result of the postsynaptic D2 receptor reduction along with preserved presynaptic activity in the nigrostriatal dopaminergic system reflects a pathophysiology of iNPH. Postsynaptic D2 receptor hypoactivity in the dorsal putamen may predict the severity of gait impairment in iNPH.
Journal of Cerebral Blood Flow & Metabolism advance online publication, 16 August 2006; doi:10.1038/sj.jcbfm.9600389

Keywords: CFT; idiopathic normal pressure hydrocephalus; positron emission tomography; raclopride; striatum

Introduction

Clinical features of normal pressure hydrocephalus (NPH) are gait disturbance, progressive dementia, and urinary incontinence, known as a clinical triad (Hakim and Adams, 1965). The NPH symptoms are thought to be a clinical entity that can be treated by surgical interventions such as shunting (Adams *et al*, 1965). The possible treatment of this disease led us to explore a surrogate marker for NPH that enables proper diagnosis at an early stage. Clinically, gait disturbance is likely the first sign and important symptom in NPH (Fisher, 1982). However, the hypokinetic type of gait disturbance is often seen in other neurologic diseases such as Parkinson's disease (PD) and dementia with extrapyramidal symptoms. Differentiating NPH from PD may be possible by observing improvement of gait velocity after withdrawal of cerebral spinal fluid (CSF) (Sudarsky and Simon, 1987) or after L-dopa treatment (Blin *et al*, 1991). However, one difficulty is that some NPH patients suffer from parkinsonism that can be ameliorated by surgical shunt (Curran and Lang, 1994). A recent case report with positron emission tomography (PET) on noncommunicating

Correspondence: Dr Y Ouchi, Positron Medical Center, Hamamatsu Medical Center, 5000 Hirakuchi, Hamamatsu 434-0041, Japan.
E-mail: ouchi@pmc.hmedc.or.jp
This research was supported by Health and Labor Sciences Research Grants.
Received 23 May 2006; revised 10 July 2006; accepted 11 July 2006

NPH patient (acqueductal stenosis) with parkinsonism showed reduction in [^{18}F]Dopa uptake in the basal ganglia, suggesting involvement of dopaminergic derangement in patients with NPH (Racette *et al*, 2004). Morphological investigations on the midbrain in secondary NPH patients favor a mechanical theory that accounts for developing parkinsonism in NPH (Jankovic *et al*, 1986; Zeidler *et al*, 1998). However, there have been no reports about the dopaminergic alterations in patients with idiopathic, communicating NPH.

Combination of a presynaptic dopamine transporter radiotracer, [^{11}C]2-β-carbomethoxy-3β-(4-fluorophenyl) tropane ([^{11}C]CFT), and a predominantly postsynaptic D2 receptor radiotracer, [^{11}C]raclopride, in PET studies allows us to evaluate presynaptic and postsynaptic dopaminergic activities in the basal ganglia (Farde *et al*, 1986; Ouchi *et al*, 1999*a*). The *in vivo* findings characteristic of early PD were an asymmetric pattern of tracer binding, that is, decreased binding of presynaptic radiotracer and normal or increased binding of postsynaptic radiotracer (Ouchi *et al*, 1999*a*), and differences in regional susceptibility (Ouchi *et al*, 1999*b*) in line with the pathologic finding (Fearnley and Lees, 1991; Kish *et al*, 1988). Likewise, it can be speculated that there will be an uneven pattern of tracers' accumulation in the dopaminergic projection areas in idiopathic communicating NPH, because morphological change of the midbrain might be related to severity of gait impairment in the disease (Lee *et al*, 2005).

The purpose of this study was to measure quantitatively the binding potentials (BPs) of [^{11}C]CFT and [^{11}C]raclopride in drug-naive patients with idiopathic normal pressure hydrocephalus (iNPH) on the same day, because any delay in the measurement of the two tracers could devalue the accurate relationship of the viability of presynaptic and postsynaptic dopaminergic neurons that might be affected by increased intraparenchymal fluid of CSF (Owler *et al*, 2004) in the living brain.

Materials and methods

Subjects

Eight patients with iNPH who were all naïve to dopaminergic drugs (five men, three women: mean age 72.4 years $\pm$4.0 s.d. (range 64 to 77)), and eight age-matched healthy subjects (six men, two women, mean age 66.9 years $\pm$ 4.5 s.d. (range 62 to 73)) participated in the current study. Diagnosis of iNPH was based on the clinical and imaging features: gait disturbance, cognitive deterioration with more or less urinary incontinence, normal lumber CSF pressure $<$20 cm H_2O (Adams *et al*, 1965; Hakim and Adams, 1965), and enlargement of the brain ventricles with some degree of deep white matter hyperintensities and reduction of the cortical sulcal space in the superior convexity on the coronal view of magnetic resonance imaging (MRI) (Kitagaki *et al*, 1998). The morphological MRI and neurologic and blood tests excluded a possibility of secondary NPH and other neurologic diseases such as progressive supranuclear palsy or corticobasal degeneration. In the present study, however, half of the patients were on medication for internal diseases (Table 1). Patient No. 3 had a small meningioma in the cerebellum, which was considered irrelevant to the NPH etiology. As shown in Table 1, no patients suffered from extrapyramidal symptoms such as rigidity or tremor but freezing, magnetic gait, cognitive decline, and some degree of difficulty in urination were observed. A CSF tap test (Wikkelso *et al*, 1986) after PET measurement was performed to support the diagnosis and introduction of shunt surgery. All medicines for their accompanying diseases were temporarily ceased 12 h before the PET measurement. All subjects were free from regular use of neuroleptic and hypnotic drugs. The current study was approved by the local Ethics Committee of the Hamamatsu Medical Center, and written informed consent was obtained from all participants after full explanation of the nature of the present study.

Psychological and Behavioral Assessments

The tests consisted of a general cognition and memory test (Mini-Mental State Examination: full score = 30); an affect

Table 1 Clinical characteristics of idiopathic normal pressure hydrocephalus patients

No.	*Age*	*Sex*	*DD*	*MMSE*	*Gait*	*UI*	*Complications*	*T2-MRI*	*Medication*	*AT*	*NT*
1	71	F	3.0	25	1	2	None	VD	None	15	18.3
2	77	F	1.2	14	2	3	None	sWM HIAs, VD	Anti-pollakiuria	6	21.0
3	76	F	1.1	24	1	2	None	VD, Cer tumor	None	8	13.0
4	71	M	0.5	23	1	3	HT, Arrhythmia	sWM & BG HIAs, VD	Anti-HT	16	14.8
5	74	M	4.0	23	2	2	None	VD	None	15	16.2
6	74	M	6.0	25	2	3	HT	sWM HIAs, VD	Anti-HT	15	14.5
7	72	M	1.1	26	1	3	HT	sWM HIAs, VD	Anti-HT	18	12.6
8	64	M	1.0	27	1	1	None	VD	None	20	13.5

DD: disease duration from onset to PET measurement (year); MMSE: mini-mental state examination; Gait: 0 = normal, 1 = insecure, 2 = insecure with any support, 3 = wheelchair; UI: urinary incontinence (0 = none, 1 = present without a diaper on, 2 = present occasionally with a diaper on, 2 = diaper requisite); VD: ventricular dilatation; sWM: subcortical white matter; HIAs: high intensity areas; BG: basal ganglia; Cer: cerebellum; SAH: subarachnoid hemorrhage; HT: hypertension; anti-HT: anti-hypertensive drug; AT: affect test with the full score of 20; NT: navigation time (second).

test in which subjects evaluate facial expressions on different cards by choosing appropriate answers from the following basic affects: happiness, sadness, surprise, disgust, anger, fear (full score = 20), and a walking test (the time required for navigating a 5-m-long path on a flat corridor both ways). Our preliminary examination showed that 11 healthy subjects (mean age = 50.4 years) scored more than 28 on the MMSE, 20 in the affect test, and took < 10 secs in the back-and-forth walk (data not shown).

Magnetic Resonance Imaging and Positron Emission Tomography Procedures

We performed three-dimensional MRI for all participants just before the PET measurement using a static magnet (0.3 T MRP7000AD, Hitachi, Tokyo, Japan) with three-dimensional mode sampling to determine the areas of the midbrain and the striatal nuclei for setting the regions of interest (ROIs) and ventricles for morphometric analysis. The MRI measures and a mobile PET gantry allowed us to generate PET images parallel to the intercommisural (ACPC) line without reslicing during image reconstruction; using this approach, we were able to allocate ROIs on the target regions of original PET images (Ouchi *et al*, 1999*b*).

For PET scans, we used a high-resolution brain-purpose SHR12000 (Hamamatsu Photonics KK, Hamamatsu, Japan) tomograph (intrinsic resolution, $2.9 \times 2.9 \times 3.4$ full-width half-maximum, 47 slices, 163 mm axial field of view). After setting the scanner's gantry parallel to the AC-PC line by tilting it, a 10-mins transmission scan for attenuation correction was performed using a $^{68}Ge/^{68}Ga$ source with the subject's head fixed by a radiosurgery purpose thermoplastic facemask, which enabled the head to be fixed to the same place between the first and second PET measurements among the same subjects. In the [^{11}C]CFT PET study, we performed serial scans (time frames: 4×30, 20×60, 14×300 secs) and periodical arterial blood sampling for 92 mins after injecting intravenously a 350-MBq dose of [^{11}C]CFT at a slow bolus taking 1 min (Ouchi *et al*, 1999*b*). To determine unchanged radioligand and radioactive metabolites, additional arterial blood samples were drawn at 1, 5, 20, 30, and 45 mins after the tracer injection and analyzed using thin-layer chromatography and a storage-phosphor-screen bioimaging analyzer (BAS-1500, Fuji Film, Tokyo, Japan). The free metabolite-corrected plasma activities were fitted to a sum of three exponentials by the nonlinear least-squares method with the nonweighted Gauss–Newton algorithm. In the [^{11}C]raclopride study, PET measurement was performed after a time interval of 3 h to allow for the decay of radioactivity. Each participant with the subject's head fixated at the same position as in the [^{11}C]CFT study underwent dynamic PET scans (4×30, 20×60, and 8×300 secs) for 62 mins after a slow bolus injection of a 300-MBq dose of [^{11}C]raclopride with periodical arterial blood sampling for metabolite correction (Ouchi *et al*, 2002).

Data Analysis

Because various types of structural alterations including ventricular enlargement existed in this iNPH group, we first made a morphometric study for morphology of the midbrain and lateral ventricle. The ventricular dilatation was evaluated by Evans index larger than 0.3 (the ratio of the longest distance between the frontal horns of the lateral ventricles to the longest diameter of the right-to-left side of the brain) (Synek *et al*, 1976). We also measured the maximum oblique diameter of the midbrain from the aqueduct via the substantia nigra to the edge of cerebral peduncle and the maximum interpeduncular distance at the level of the substantia nigra and red nucleus (Doraiswamy *et al*, 1992; Ouchi *et al*, 2005), and the size of frontal horn of the lateral ventricle (O'Hayon *et al*, 1998) on the MR images. All morphometric values *except* for Evans index were expressed as ratios (percentage) to the maximal diameter between the frontal and occipital poles along the intercommissural line.

Then, multiple irregular ROIs (40 to 200 mm^2) were drawn bilaterally over the nucleus accumbens, ventromedial striatum (head of the caudate), the inferolateral (ventral putamen) and superodorsal parts (dorsal putamen) of the striatum, and the cerebellum on the MR images (Mai *et al*, 1997). These ROIs were then transferred onto the corresponding dynamic [^{11}C]CFT and [^{11}C]raclopride images with 6.8-mm slice-thickness data generated after adding two consecutive slices using image-processing software (Dr View, Asahi Kasei Co., Tokyo, Japan) on a SUN workstation (Hypersparc ss-20, SUN Microsystems, San Diego, CA, USA) (Ouchi *et al*, 1999*b*). A brain morphological change because of ventricular enlargement may cause an error of parameter estimation due to partial volume effect. However, this method of determining the ROIs based on individual MRI minimized the error and the pitfalls of applying a standardized normal brain template to the anatomically affected NPH brain (Owler *et al*, 2004; Giovacchini *et al*, 2005). Indeed, we performed a morphometric analysis for the ROI volumes to test any difference in volume because of the presence of structural atrophy in iNPH. A simple *t*-test revealed no significant difference in volume between the two groups (see Table 3). The values of bilateral ROIs for the cerebellum in the disease group and for all the regions examined in the control group were averaged for further analysis.

Because, as described in the PET procedure, participants were scanned in the same position between the two PET measurements, the same ROIs could be placed on both [^{11}C]CFT and [^{11}C]raclopride parametric images. This approach allowed us to examine both aspects of dopaminergic functions presynaptically and postsynaptically *in vivo*. The *BP*, B_{max}'/k_d (or k_3/k_4) for [^{11}C]CFT was estimated based on the three-compartment model by fitting artery and tissue TACs for blood-brain barrier transport rates (K_1), the free plus nonspecific distribution volume (DV) (K_1/k_2), and the binding and dissociation rate constants (k_3 and k_4 respectively), as described elsewhere (Ouchi *et al*, 1999*a*). In addition, the BP for [^{11}C]raclopride was estimated using the following equation and the nonlinear least-squares fitting method; B_{max}'/k_d = (target